Article

Molecular Cell

Identification of an RNA Polymerase III Regulator Linked to Disease-Associated Protein Aggregation

Graphical Abstract

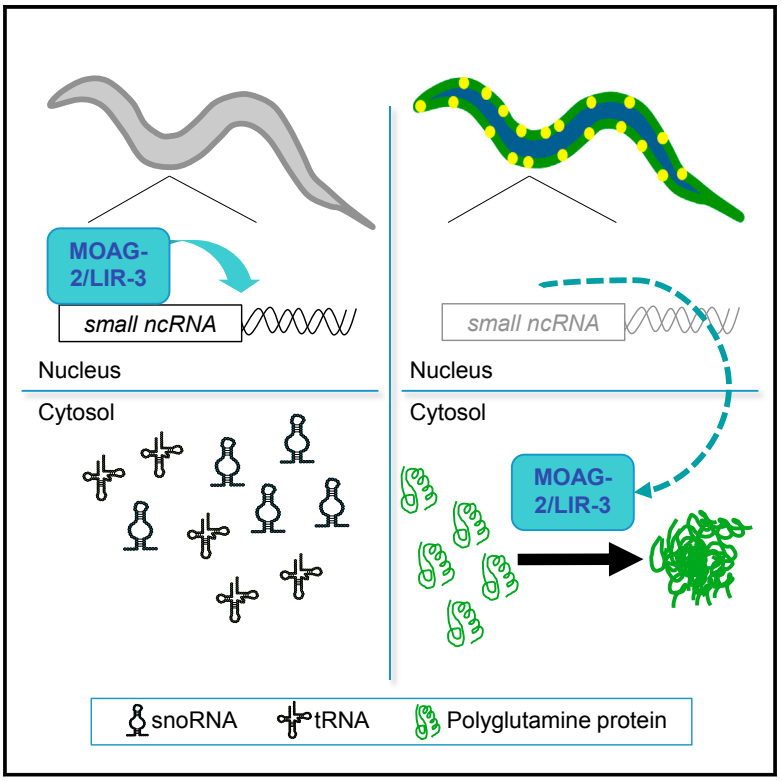

Authors

Olga Sin, Tristan de Jong, Alejandro Mata-Cabana, ..., Valerie Reinke, Victor Guryev, Ellen A.A. Nollen

Correspondence

v.guryev@umcg.nl (V.G.), e.a.a.nollen@umcg.nl (E.A.A.N.)

In Brief

The cellular mechanisms that drive polyglutamine aggregation are poorly understood. Sin et al. show that polyglutamine relocates MOAG-2/LIR-3 from the nucleus to the cytosol, thereby converting this protein into an aggregation-promoting factor to drive protein aggregation and toxicity.

Highlights

- Inactivation of MOAG-2/LIR-3 reduces polyglutamine aggregation
- MOAG-2/LIR-3 regulates Pol III-mediated transcription of small non-coding RNAs
- Polyglutamine mislocalizes MOAG-2/LIR-3 from the nucleus to the cytosol
- Polyglutamine converts MOAG-2/LIR-3 into an aggregation-promoting factor

Sin et al., 2017, Molecular Cell 65, 1096–1108
March 16, 2017
http://dx.doi.org/10.1016/j.molcel.2017.02.022

CellPress

CellPress

Molecular Cell
Article

Identification of an RNA Polymerase III Regulator Linked to Disease-Associated Protein Aggregation

Olga Sin,[1,2] Tristan de Jong,[1] Alejandro Mata-Cabana,[1] Michelle Kudron,[3] Mohamad Amr Zaini,[1] Francesco A. Aprile,[5] Renée I. Seinstra,[1] Esther Stroo,[1] Roméo Willinge Prins,[1] Céline N. Martineau,[1] Hai Hui Wang,[1] Wytse Hogewerf,[1] Anne Steinhof,[4] Erich E. Wanker,[4] Michele Vendruscolo,[5] Cornelis F. Calkhoven,[1] Valerie Reinke,[3] Victor Guryev,[1,*] and Ellen A.A. Nollen[1,6,*]

[1]European Research Institute for the Biology of Ageing, University of Groningen, University Medical Centre Groningen, 9700 AD Groningen, the Netherlands

[2]Graduate Program in Areas of Basic and Applied Biology, Instituto de Ciências Biomédicas Abel Salazar, Universidade do Porto, 4050-313 Porto, Portugal

[3]Department of Genetics, Yale University School of Medicine, New Haven, CT 06520, USA

[4]Max Delbrück Center for Molecular Medicine, 13125 Berlin, Germany

[5]Department of Chemistry, University of Cambridge, Cambridge CB2 1EW, UK

[6]Lead Contact

*Correspondence: v.guryev@umcg.nl (V.G.), e.a.a.nollen@umcg.nl (E.A.A.N.)

http://dx.doi.org/10.1016/j.molcel.2017.02.022

SUMMARY

Protein aggregation is associated with age-related neurodegenerative disorders, such as Alzheimer's and polyglutamine diseases. As a causal relationship between protein aggregation and neurodegeneration remains elusive, understanding the cellular mechanisms regulating protein aggregation will help develop future treatments. To identify such mechanisms, we conducted a forward genetic screen in a *C. elegans* model of polyglutamine aggregation and identified the protein MOAG-2/LIR-3 as a driver of protein aggregation. In the absence of polyglutamine, MOAG-2/LIR-3 regulates the RNA polymerase III-associated transcription of small non-coding RNAs. This regulation is lost in the presence of polyglutamine, which mislocalizes MOAG-2/LIR-3 from the nucleus to the cytosol. We then show biochemically that MOAG-2/LIR-3 can also catalyze the aggregation of polyglutamine-expanded huntingtin. These results suggest that polyglutamine can induce an aggregation-promoting activity of MOAG-2/LIR-3 in the cytosol. The concept that certain aggregation-prone proteins can convert other endogenous proteins into drivers of aggregation and toxicity adds to the understanding of how cellular homeostasis can be deteriorated in protein misfolding diseases.

INTRODUCTION

Neurodegenerative disorders such as Alzheimer's, Parkinson's, and Huntington's diseases represent a major health problem and demand a better understanding of the molecular mechanisms of pathogenesis in order to develop disease-modifying treatments. The hallmark of many neurodegenerative disorders is the presence of protein aggregates in different brain areas of affected patients (Soto, 2003). These insoluble macromolecular structures are enriched in aggregation-prone proteins that—by exposing certain regions of their amino acid sequences—associate in an aberrant manner with other proteins, thereby hampering normal cellular function (Eisenberg and Jucker, 2012; Olzscha et al., 2011; also reviewed in Chiti and Dobson, 2009; Sin and Nollen, 2015). It is not yet clear, however, whether these protein aggregates are actually a cause or a consequence of the disease. The current view is that the soluble precursors of these aggregates—in particular some oligomeric forms—are the main cytotoxic species, and that at least in some cases the aggregation process can represent a protective measure to sequester these smaller harmful species (Arrasate et al., 2004; Bolognesi et al., 2010; Kayed et al., 2003; Miller et al., 2011).

These observations focus the attention on the cellular factors that can drive protein aggregation, which are currently poorly understood. In some cases, direct aggregation-promoting factors have been identified, both in humans and in animal models, and include SH3GL3 (Davranche et al., 2011; Sittler et al., 1998), MOAG-4/SERF (Falsone et al., 2012; van Ham et al., 2010), and UNC-30 (Garcia et al., 2007). More studies, however, are needed to acquire a more comprehensive understanding of this phenomenon.

In this context, the roundworm *C. elegans* is a much-used animal model for neurodegenerative diseases and is proving very useful in providing a basic understanding of protein aggregation. If we can use this model organism to identify genetic modifiers of protein aggregation, then we can also obtain insight into the cellular pathways that are dysregulated in the pathogenesis of human protein misfolding diseases and target them for pharmacological intervention. Indeed, a wide variety of genetic screens have already been performed in *C. elegans* to find genes that regulate protein aggregation and its associated toxicity (Hamamichi et al., 2008; Kuwahara et al., 2008; Lejeune et al., 2012; Nollen et al., 2004; Silva et al., 2011; van der Goot et al., 2012; van Ham et al., 2010). The aim of the current study is to identify genes that drive protein aggregation, to discover the function of

such genes, and to understand how they are related to protein aggregation. We identified MOAG-2/LIR-3 as a modifier of aggregation, since this protein in the presence of polyglutamine shifts its role from a transcriptional regulator of small non-coding RNAs (ncRNAs) to an aggregation and toxicity promoting factor.

RESULTS

Inactivation of MOAG-2/LIR-3 Reduces Polyglutamine Aggregation

To identify genes whose products are capable of driving protein aggregation, we performed a forward genetic screen in a *C. elegans* model in which the body-wall muscle cells express a transgene consisting of an aggregation-prone polyglutamine stretch of 40 residues fused to YFP (Q40-YFP) (van Ham et al., 2010). We screened for mutants with reduced polyglutamine aggregation, and we named the resulting genes "modifiers of aggregation" (*moag*) (van Ham et al., 2010). At the fourth larval stage (L4), *moag-2(pk2183)* (hereafter designated as *moag-2/lir-3(pk2183)*) showed a reduction of about 50% in the number of aggregates relative to the wild-type Q40 worms (Figures 1A, 1B, and S1A). SNP mapping and genome sequencing allowed us to fine-map the causal mutation and revealed six genes as putative candidates for *moag-2* (Figure S1B). For one of these, which mapped to *lir-3* (lin-26 related; sequence: F37H8.1; GenBank: NM_063994), the causative mutation was in the start codon, replacing the first methionine with an isoleucine (Met1Ile) (Figures 1C and S1B).

The *lir-3* gene encodes a LIN-26-like zinc-finger protein of unknown function (http://www.wormbase.org/, June 2016). It is predicted to have two zinc-finger domains of the C2H2 type (residues 191–214 and 224–247) at the carboxyl terminus and a nuclear localization signal spanning amino acid residues 132–141 (http://nls-mapper.iab.keio.ac.jp/, June 2016) (Figure S1C). LIR-3 shares two non-canonical C2H2 zinc-finger motifs with three other *C. elegans* proteins: LIN-26 (31%–35% similarity), LIR-1 (20%–31% similarity), and LIR-2 (25% similarity) (Dufourcq et al., 1999).

To assess whether *moag-2* was *lir-3*, we used an *lir-3(tm813)* deletion mutant (hereafter designated as "*moag-2/lir-3(tm813)*") and crossed it with the polyglutamine (Q40) worm model. This strain has a 795 bp deletion spanning residues 276–1,070 of the F37H8.1 sequence that also causes a premature stop codon (Figures 1C and S1C). This partial deletion of *lir-3* caused a 35% reduction of aggregates relative to the numbers seen in wild-type worms (Figure 1D). Worms heterozygous for *lir-3* deletion allele had aggregate numbers similar to those seen in the wild-type, suggesting that the reduction of aggregation was recessive and due to the loss of function of *lir-3* (Figure 1D). We next asked whether overexpression of *lir-3* could restore the aggregation phenotype. To this end, we injected worms with a rescue fragment, consisting of full-length *lir-3*, including a 1.5 kb sequence upstream of the start codon to include its endogenous promoter as well as 330 bp downstream to include the 3′ UTR (Figure 1C). Expression of the *lir-3* rescue fragment in Q40; *lir-3(tm813)* worms was able to restore the aggregation phenotype by 2-fold ($p < 0.001$), confirming *lir-3* as a gene responsible for driving aggregation in the polyglutamine model (Figures 1E and S1D). Taken together, these results demonstrate that *lir-3* is *moag-2*.

A specific property of protein aggregates in the brains of neurodegenerative disease patients that is also captured by the *C. elegans* polyglutamine model used here is that they are typically insoluble in strong detergents such as sodium dodecyl sulfate (SDS) (Lee et al., 1999; Shankar et al., 2008; Yanamandra et al., 2015). To establish whether MOAG-2/LIR-3 promoted aggregation of SDS-insoluble polyglutamine aggregates, we performed a filter retardation assay on lysates of wild-type and *moag-2/lir-3* mutant polyglutamine worms (Scherzinger et al., 1997; Wanker et al., 1999). This assay enables the detection of SDS-insoluble protein aggregates, while soluble species are not captured. Both Q40;*moag-2/lir-3(pk2183)* and Q40;*moag-2/lir-3(tm813)* mutants had fewer SDS-insoluble aggregates than their corresponding Q40 controls (Figure 1F). The reduction of SDS-insoluble aggregates was more pronounced in the point mutant (43%; $p = 0.05$) than in the deletion mutant (26%; $p = 0.18$) (Figure S1E). Mutation or partial deletion of *moag-2/lir-3* did not cause a discernible reduction in the transcription or the protein expression level of Q40-YFP, indicating that *moag-2/lir-3* does not reduce aggregation by reducing expression levels of the Q40-YFP protein (Figures 1F and 1G). Together, these results indicate that *moag-2/lir-3* drives the formation of SDS-insoluble polyglutamine aggregates.

MOAG-2/LIR-3 Is a C2H2-Domain Protein Associated with RNA Polymerase III Promoters

Having established that mutation of *moag-2/lir-3* reduces polyglutamine aggregation, we next determined the endogenous function of the corresponding protein. C2H2 zinc-finger domains are predominantly associated with DNA-binding transcription factors but may also have other functions such as mediating protein-protein interactions or binding to RNA (Brown, 2005; Hall, 2005; Krishna et al., 2003). Bioinformatics analysis combined with manual curation predicted MOAG-2/LIR-3 to be a transcription factor (Reece-Hoyes et al., 2005, 2007). To explore this possibility, we determined the subcellular localization of FLAG-tagged MOAG-2/LIR-3 protein in wild-type N2 worms. Indirect immunofluorescence using an anti-FLAG antibody revealed that MOAG/LIR-3 is localized in the nucleus (Figures 2A and S2A).

Next, we performed chromatin immunoprecipitation followed by deep sequencing (ChIP-seq) in L4-staged worms that expressed an integrated construct of *lir-3* fused to FLAG and GFP (Sarov et al., 2012; Zhong et al., 2010). This analysis yielded a total of 678 unique MOAG-2/LIR-3 binding sites, 404 of which overlapped with 813 *C. elegans* genes. Further analyses of these genes revealed that MOAG-2/LIR-3 binding was enriched in the transcription start sites (TSSs) of tRNA genes (35.7%, $p < 0.001$), small nucleolar RNA (snoRNA) genes (6.3%, $p < 0.001$), rRNA genes (2.5%, $p < 0.001$), and small nuclear RNA (snRNA) genes (2.2%, $p < 0.002$) (Figures 2B and S2B). While MOAG-2/LIR-3 was also found in the vicinity of protein-coding and other ncRNA genes, this binding was not significantly enriched (Figures 2B, 2C, and S2B).

We then asked whether the binding sites were enriched in any consensus sequence motif that could be recognized by

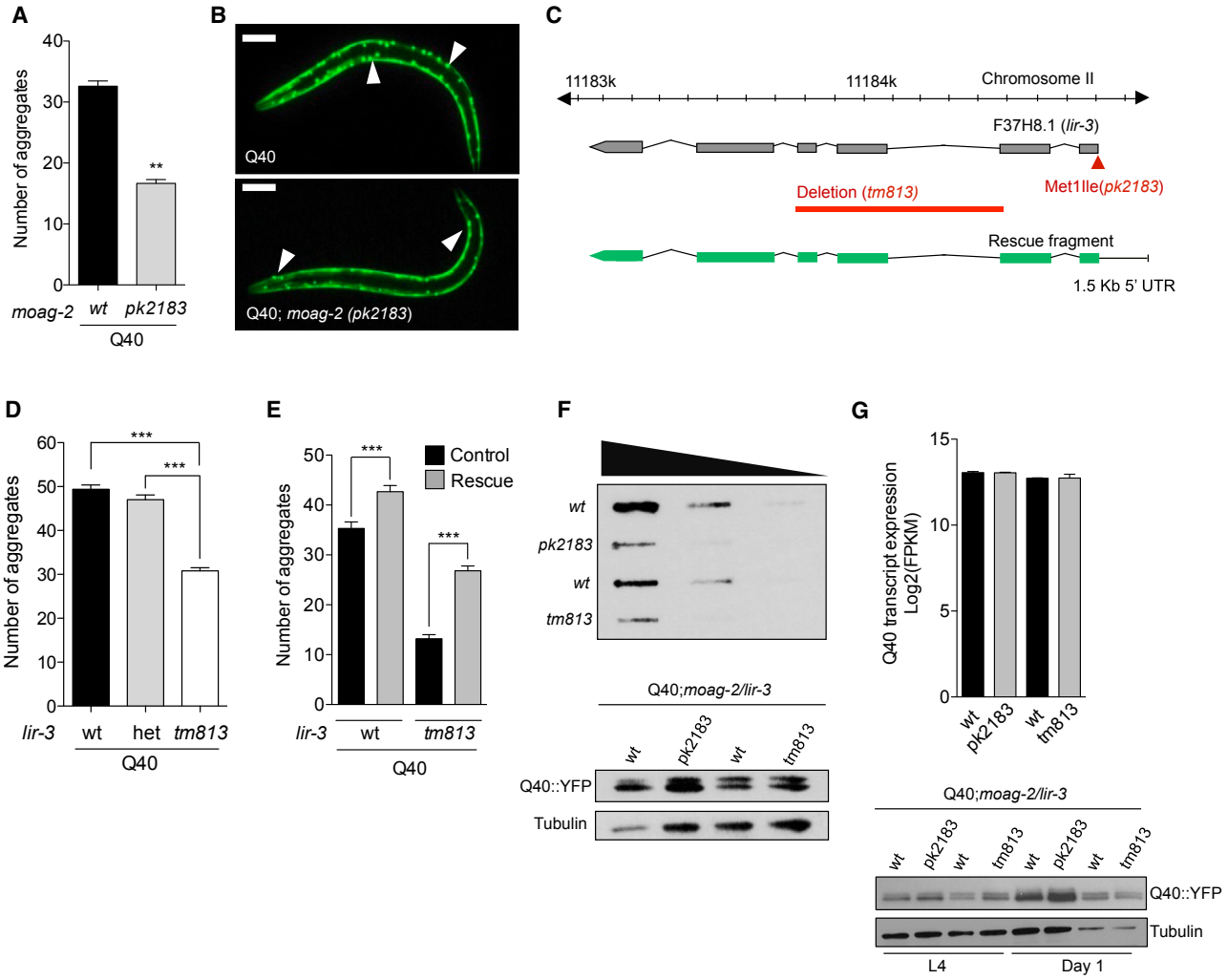

Figure 1. Identification of *moag-2/lir-3* as an Aggregation-Promoting Factor

(A) Number of aggregates in Q40 worms and Q40;*moag-2(pk2183)* worms.

(B) Representative images of Q40 worms and Q40;*moag-2(pk2183)* worms. Scale bar, 75 μm. See also Figure S1A.

(C) Chromosomal location of *lir-3* (F37H8.1, chromosome II, reverse strand of assembly; http://www.wormbase.org, WS248), showing the point mutation in the start codon (red arrow), the partial deletion (red bar), and the rescue fragment (green). See also Figures S1B and S1C.

(D) Number of aggregates in Q40 worms with either wild-type alleles, or heterozygous (het) or homozygous (tm813) deletion for the *lir-3(tm813)* allele.

(E) Number of aggregates in Q40 worms and Q40;*lir-3*(*tm813*) worms, with and without transgenic overexpression of an injected *lir-3* rescue fragment, including its endogenous promoter. See also Figure S1D.

(F) Filter retardation assay with 5-fold serial dilutions of crude protein extract from Q40 worms and Q40;*moag-2/lir-3* mutant worms. The results shown are from a representative experiment of three biological replicates. Q40-YFP and α-tubulin expression were included as controls. See also Figure S1E.

(G) Q40-YFP transcript expression detected by RNA sequencing in L4-stage worms and protein expression detected in urea-treated L4-stage worms and day 1 adult worms.

In all panels, aggregate counting, representative images, and filter retardation assay were performed at the L4 stage and the average of three biological replicates is represented. Data are represented as mean ± SEM and significance was calculated using a one-tailed unpaired Student's t test. **$p < 0.01$; ***$p < 0.001$.

MOAG-2/LIR-3. Of the 678 binding sites initially identified in our ChIP-seq data, more than half of the sites contained Box A and Box B sequence motifs, 301 of which contained both motifs (Figures 2D and 2E). Box A and Box B constitute the canonical type 2 promoter site recognized by the RNA polymerase (Pol) III complex (Ikegami and Lieb, 2013; Schramm and Hernandez, 2002). Pol III is responsible for the transcription of structural or catalytic snRNAs, of tRNAs, and of snoRNAs, which mediate chemical modifications of other RNA molecules (Bratkovič and Rogelj, 2014; Guthrie and Patterson, 1988; Schramm and Hernandez, 2002; White, 2011). These findings led us to hypothesize that MOAG-2/LIR-3 may bind to the same target promoters as Pol III. Binding in the proximity of non-coding genes has been shown on occasion for several *C. elegans* transcription factors, including PHA-4, PQM-1, and GEI-11 (Niu et al., 2011). These observations prompted us to ask whether the association

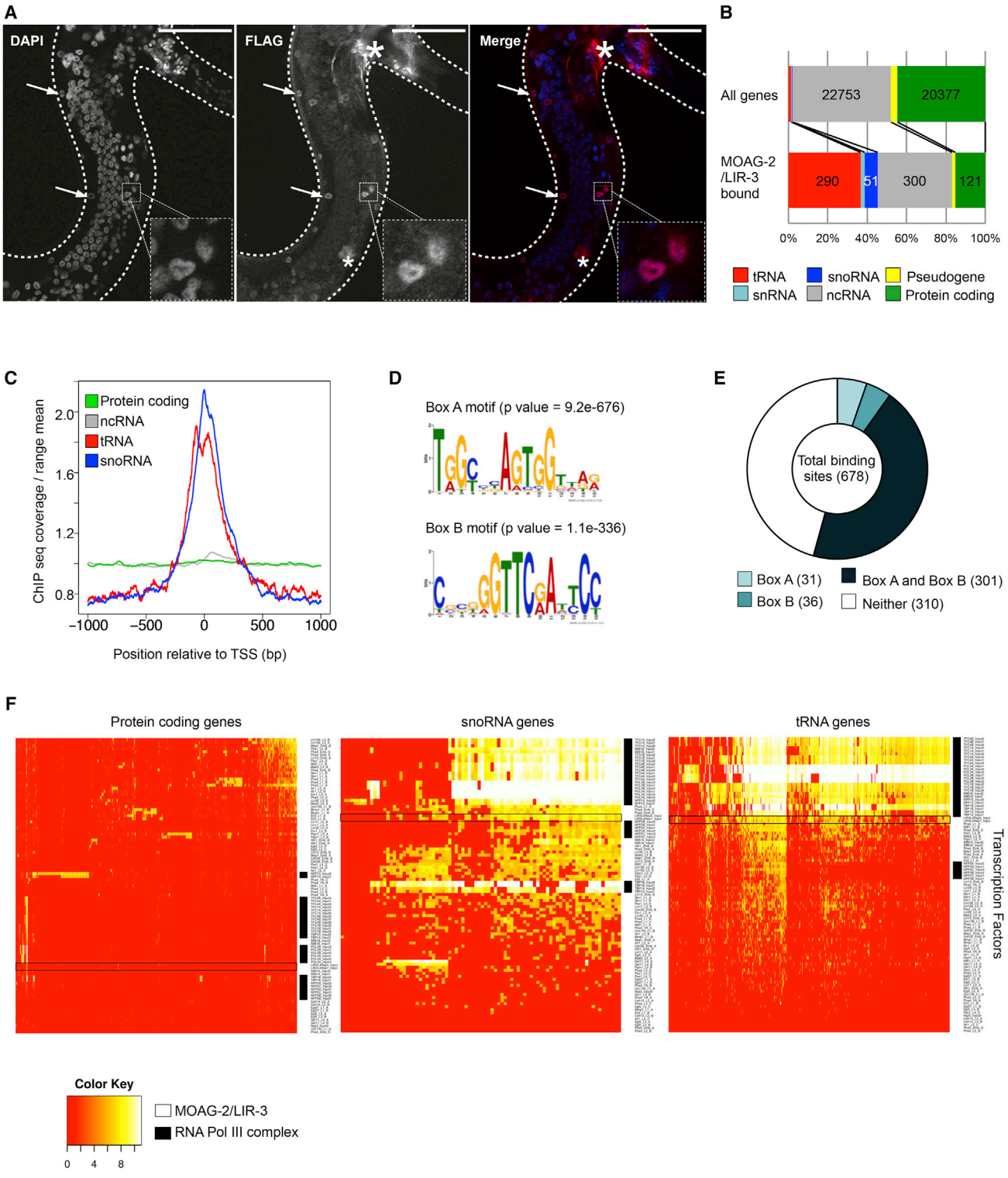

Figure 2. MOAG-2/LIR-3 Preferentially Binds to Promoters of Small ncRNAs

(A) Subcellular localization of MOAG-2/LIR-3 in wild-type N2 worms. Scale bar, 50 μm. Arrowheads point at nuclei; asterisk is non-specific staining. See also Figure S2A.

(B) Enrichment of binding of MOAG-2/LIR-3 to different gene biotypes (1 kb upstream/downstream of TSS) relative to genes distributed genome-wide. See also Figure S2B.

(legend continued on next page)

between MOAG-2/LIR-3 and the Pol III complex resembled the binding of these transcription factors to the promoters of non-coding genes. To answer this question, we collected publicly available ChIP-seq data for known *C. elegans* transcription factors (http://www.modencode.org, September 2014) and analyzed binding to the promoters of protein-coding genes, snoRNA genes, and tRNA genes (Figure 2F). While there is little association between MOAG-2/LIR-3 and the promoters of protein-coding genes, the MOAG-2/LIR-3 binding profile is very similar to that of a group of clustered factors that contain representative components of the Pol III complex. These factors include Pol III, TATA binding protein (TBP-1), two subunits of the transcription factor for Pol III C (TFC-1 and TFC-4), and the nuclear pore proteins NPP-3 and NPP-13, which have recently been shown to associate with the Pol III complex to regulate tRNA and snoRNA splicing (Ikegami and Lieb, 2013). In contrast to the majority of the other transcription factors, the binding of these factors is very abundant in the promoters of snoRNAs and of tRNAs (Figure 2F). Therefore, the binding of MOAG-2/LIR-3 to the promoters of small ncRNA genes suggests that MOAG-2/LIR-3 is associated with Pol III transcription.

MOAG-2/LIR-3 Is a Positive Regulator of Pol III-Mediated Transcription of Small ncRNAs

Because we found MOAG-2/LIR-3 to bind to the promoters of small ncRNA genes, we next asked what consequences this binding had for the transcription of Pol III downstream targets. We therefore used transcriptome profiling to compare RNA expression in wild-type worms with that in *moag-2/lir-3* mutant worms. In line with the absence of MOAG-2/LIR-3 at RNA Pol II promoter sites, we did not find any protein-coding genes that were differentially expressed between the mutants and wild-type N2 worms, thereby excluding MOAG-2/LIR-3 as a transcriptional regulator of protein-coding genes (Figures 3A and S3A). Mutations in *moag-2/lir-3*, however, did result in the downregulation of snRNAs ($p < 0.001$), snoRNAs ($p < 0.001$), and tRNAs ($p < 0.001$) in both mutants, demonstrating that MOAG-2/LIR-3 regulates Pol III-mediated transcription of these small ncRNAs (Figures 3A and S3A).

We next asked where in the TSS region MOAG-2/LIR-3 was positioned relative to the Pol III complex. To this end, we compared the positions of the ChIP-seq signals of MOAG-2/LIR-3 with those of the different components of the Pol III complex. For both the tRNA and snoRNA genes, all factors localized to the Box A- and Box B-containing promoter region, consistent with previous reports (Figures 3B, 3C, and S3B) (Ikegami and Lieb, 2013). MOAG-2/LIR-3 was also positioned at these same sites (Figures 3B and 3C).

Next, we tested whether MOAG-2/LIR-3 interacts physically with the Pol III complex by means of immunoprecipitation experiments. We found that FLAG-tagged MOAG-2/LIR-3 protein co-immunoprecipitated with Pol III, but not detectably with Pol II, confirming that MOAG-2/LIR-3 cooperates with the Pol III machinery to drive transcription of small ncRNAs (Figures 3D and S3C). The fact that MOAG-2/LIR-3 did not detectably co-immunoprecipitate with Pol II further supports the notion that MOAG-2/LIR-3 is not directly involved in the transcription of protein-coding genes (Figure 3D).

Together these results indicate that MOAG-2/LIR-3 functions as a positive regulator of the Pol III-mediated transcription of small ncRNAs in *C. elegans*.

Regulation of Protein Aggregation by MOAG-2/LIR-3 Is Independent of Its Role as a Transcriptional Regulator

Next, we asked whether MOAG-2/LIR-3 regulated protein aggregation via the Pol III-mediated transcription of small ncRNAs. We therefore used RNAi to knock down, one by one, the individual components of the Pol III complex in both wild-type worms and *moag-2/lir-3(pk2183)* mutants. To confirm RNAi knockdown, we also looked for RNAi-associated phenotypes other than aggregation. If Pol III-mediated transcription were involved in promoting protein aggregation, this would result in a reduction in the amount of aggregates in the wild-type Q40 worms, but not in the *moag-2/lir-3* mutants. However, knockdown of Pol III, TBP-1, or TFC-1 did not alter aggregation in the Q40 worms or in the Q40;*moag-2/lir-3* mutant strains, indicating that in the absence of *moag-2/lir-3* it is not the resulting lack of Pol III-mediated transcription that is responsible for the reduction in aggregation (Figures 4A, S4A, and S4B).

The nuclear pore protein *npp-13* has been shown to interact with the Pol III complex and regulate the processing of small ncRNAs (Ikegami and Lieb, 2013). The aggregation phenotype was not altered by knockdown of *npp-13* or of tRNA-processing enzymes, indicating that neither small RNA processing nor the availability of mature tRNAs is involved in reducing aggregation (Figures 4A, 4B, and S4A–S4C). These results indicate that the regulation of protein aggregation by MOAG-2/LIR-3 is separate from its involvement in RNA transcription together with the Pol III complex.

Polyglutamine Suppresses Transcription of Small ncRNAs

We next asked why the involvement of MOAG-2/LIR-3 in driving protein aggregation is independent of its role as a transcriptional regulator. We therefore first compared the RNA expression profiles of wild-type Q40 worms with those of *moag-2/lir-3* mutant Q40 worms. In contrast to wild-type N2 worms, there was no longer a reduction in the relative expression levels of the small ncRNAs in the presence of polyglutamine (Figures 4C and S4D). When we then measured the absolute levels of all RNAs, we found that in contrast to the protein-coding RNAs, pseudogenes, and other ncRNAs, the expression of snRNAs, snoRNAs, and tRNAs was already strongly reduced in wild-type Q40

(C) MOAG-2/LIR-3 binding sites within −1,000 and +1,000 bp of TSS for protein-coding, ncRNA, tRNA, and snoRNA genes.
(D) Enriched consensus DNA motifs for MOAG-2/LIR-3 with p value.
(E) Number of MOAG-2/LIR-3 binding sites containing Box A and Box B.
(F) Heatmap showing the binding of different transcription factors to *C. elegans* promoters of protein-coding, snoRNA, and tRNA genes. The hierarchical clustering was generated using the average linkage cluster method with a binary metric distance.

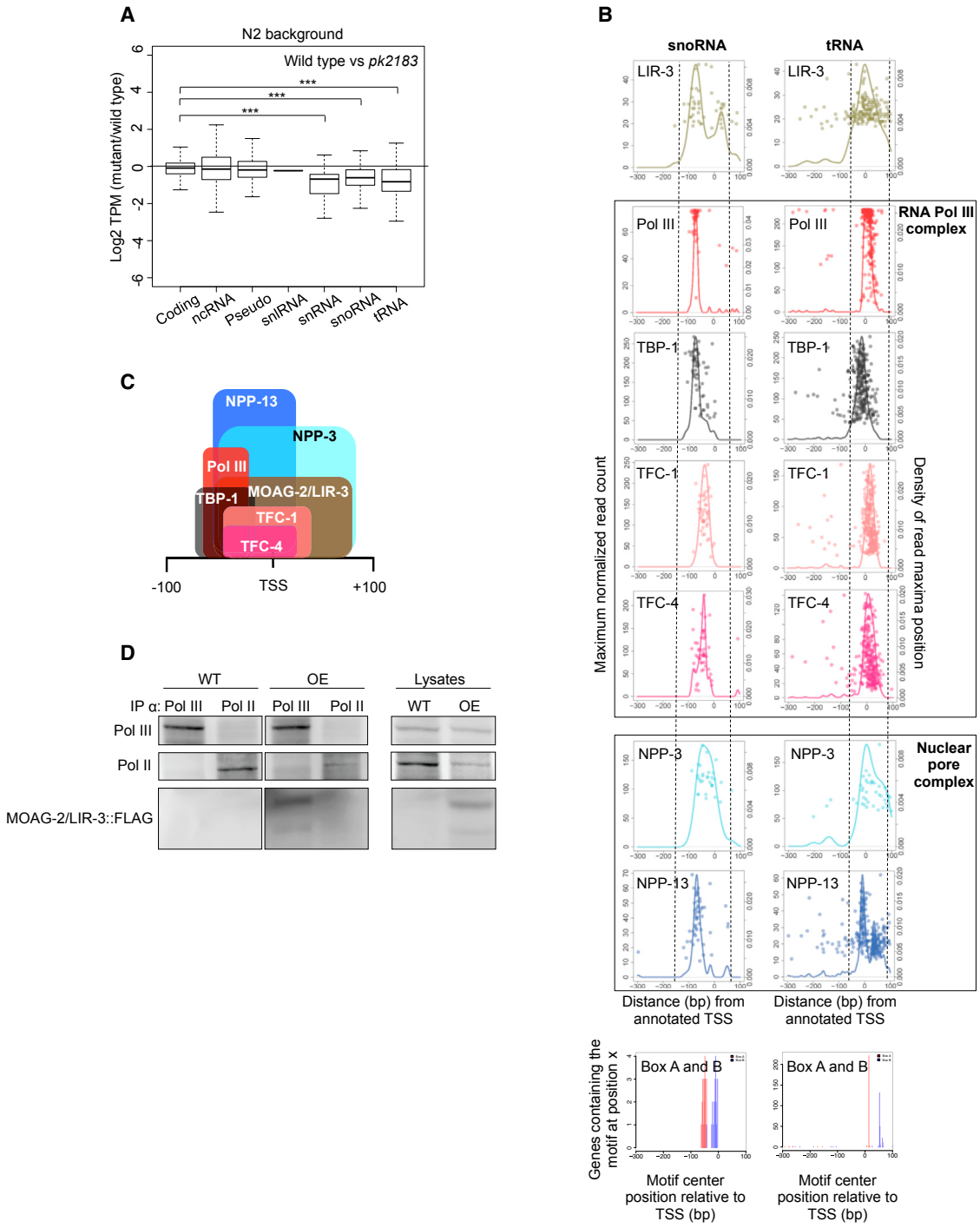

Figure 3. MOAG-2/LIR-3 Regulates Transcription of Small ncRNAs

(A) Boxplot showing the relative expression of different gene biotypes in *moag-2/lir-3(pk2183)* worms relative to the wild-type N2 background. TPM, tags per kilobase million; Coding, protein-coding genes; ncRNA, non-coding RNA; Pseudo, pseudogenes; snRNA, small nuclear RNA; snlRNA, snRNA-like RNA; snoRNA, small nucleolar RNA; tRNA, transfer RNA. The average of three biological replicates is represented and significance was calculated using a two-tailed unpaired Student's t test. ***$p < 0.001$. See also Figure S3A.

(B) Positions of ChIP-seq signal maxima relative to TSS (right y axis) with maximum normalized read count (left y axis) for the 51 snoRNA genes and the 290 tRNA genes picked in this study. Bottom box represents the motif position of Box A and Box B relative to snoRNA and tRNA genes. See also Figures S3B and S3C.

(C) Diagram showing the positions of the Pol III factors and that of MOAG-2/LIR-3 as estimated from the data presented in (B).

(D) Co-immunoprecipitation of FLAG-tagged MOAG-2/LIR-3 protein by α-Pol II and α-Pol III protein antibodies. IP, immunoprecipitation; WT, wild-type; OE, MOAG-2/LIR-3 overexpression.

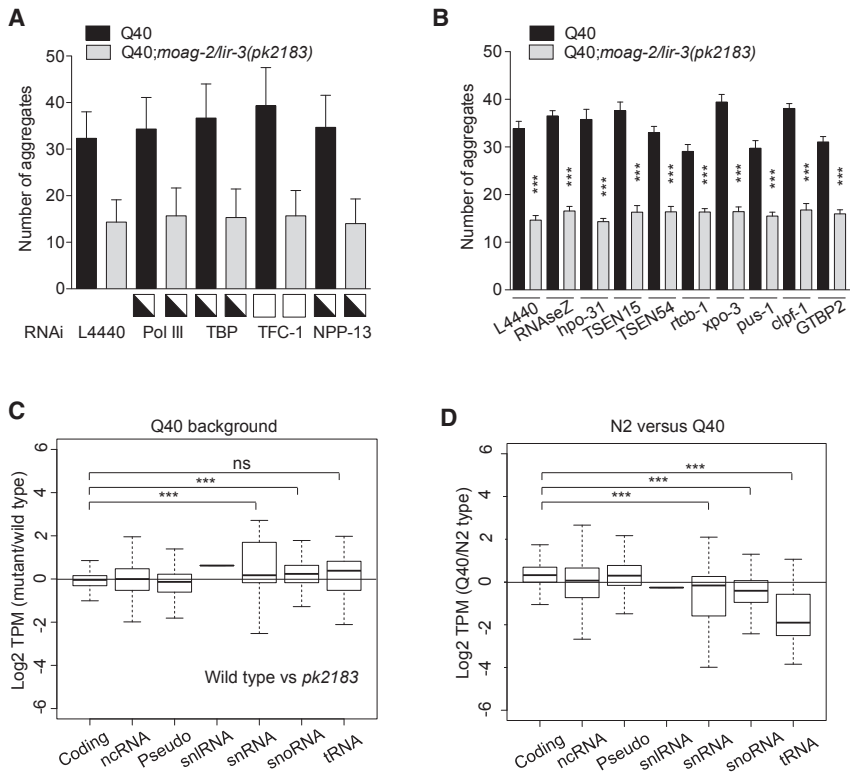

Figure 4. Polyglutamine Reduces the Transcription of Small ncRNAs

(A) Number of aggregates measured in Q40 and Q40;*moag-2/lir-3(pk2183)* worms after RNAi knockdown of individual components of the Pol III complex. As an internal quality control for RNAi, squares indicate penetrance (50% [half-open] and 0% [open]) of all associated visible RNAi phenotypes other than aggregation. See also Figures S4A and S4B.

(B) Number of aggregates measured in Q40 and Q40;*moag-2/lir-3(pk2183)* worms upon RNAi knockdown of tRNA-processing enzymes. See also Figure S4C.

(C and D) Boxplot showing the relative expression of different gene biotypes in Q40 and Q40;*moag-2/lir-3(pk2183)* worms (C) and in N2 and Q40 wild-type worms (Q40 wild-type outcrossed from *pk2183*) (D). TPM, tags per kilobase million; Coding, protein-coding genes; ncRNA, non-coding RNA; Pseudo, pseudogenes; snRNA, small nuclear RNA; snlRNA, snRNA-like RNA; snoRNA, small nucleolar RNA; tRNA, transfer RNA. See also Figures S4D and S4E.

In (A) and (B), aggregate counting was performed at the L4 stage and the average of three biological replicates is represented. Data are represented as mean ± SEM. In (C) and (D), the average of three biological replicates is represented and significance was calculated using a two-tailed unpaired Student's t test. ***$p < 0.001$; ns is not significant. See also Figures S4D and S4E.

worms ($p < 0.001$; Figures 4D and S4E). These findings explained why mutations in *moag-2/lir-3* could no longer reduce expression in these Q40 worms (Figures 4C and S4D) and indicated that presence of polyglutamine results in downregulation of small ncRNA expression.

MOAG-2/LIR-3 Increases Polyglutamine Toxicity

Having identified MOAG-2/LIR-3 as a regulator of polyglutamine aggregation, we asked whether it regulates the toxicity of polyglutamine as well. To answer to this question, we compared the motilities of worms with or without overexpression of FLAG-tagged MOAG-2/LIR-3 in absence or presence of polyglutamine over the course of 12 days. In absence of polyglutamine, FLAG-tagged MOAG-2/LIR-3 had no effect on the motility of young adults but improved the motility of old adult animals (Figure 5A). In contrast, in worms expressing polyglutamine, overexpression of MOAG-2/LIR-3 accelerated the age-dependent decline in motility (Figure 5B). To note, a deletion in *moag-2/lir-3* had no significant effect on the motility of polyglutamine worms up to 13 days of adulthood (Figure S5A). Our results with the MOAG-2/LIR-3-overexpressing worms imply that the effect of a deletion may not have been strong enough to be detected in our assays because they indicate that increasing the levels of MOAG-2/LIR-3 enhances the toxicity of polyglutamine.

MOAG-2/LIR-3 Can Directly Drive Polyglutamine Aggregation

Our results indicate that MOAG-2/LIR-3 regulates protein aggregation independently of its role in small ncRNA transcription and processing. A possible mechanism by which loss of MOAG-2/LIR-3 could suppress aggregation indirectly could be by increasing the cellular folding capacity. The transcription of protein-coding genes was not affected, however, indicating that increased transcription of folding genes was not involved (Table S3). Alternatively, MOAG-2/LIR-3 may normally sequester folding factors, which then may be released in the Q40;*moag-2/lir-3* mutants, a mechanism that has been previously proposed for an increase in protein aggregation by temperature-sensitive mutant proteins (Gidalevitz et al., 2006). If such a mechanism would be responsible for the suppression of aggregation in the Q40;*moag-2/lir-3* mutants, knockdown of folding factors in these animals would increase aggregation again. To test this possibility, we knocked down by RNAi several folding factors that have been previously shown to regulate polyglutamine aggregation (Hsu et al., 2003; Nillegoda et al., 2015; Nollen et al., 2004; Rampelt et al., 2012). The depletion of these factors could not revert the aggregation phenotype in the Q40;*moag-2/lir-3* mutants (Figure S5B). These results suggest that suppression of protein aggregation by inactivation of MOAG-2/LIR-3 is not caused by an increase in the expression or a release of folding factors.

Another possibility is that MOAG-2/LIR-3 drives aggregation directly. Precedents for aggregation-promoting factors include MOAG-4/SERF, which can drive aggregation of a variety of disease proteins via a transient direct interaction with early aggregation intermediates (Davranche et al., 2011; Falsone et al., 2012; Sittler et al., 1998; van Ham et al., 2010). To determine whether MOAG-2/LIR-3 can drive aggregation directly, we incubated GST-tagged *huntingtin* exon 1 containing 48 CAG repeats

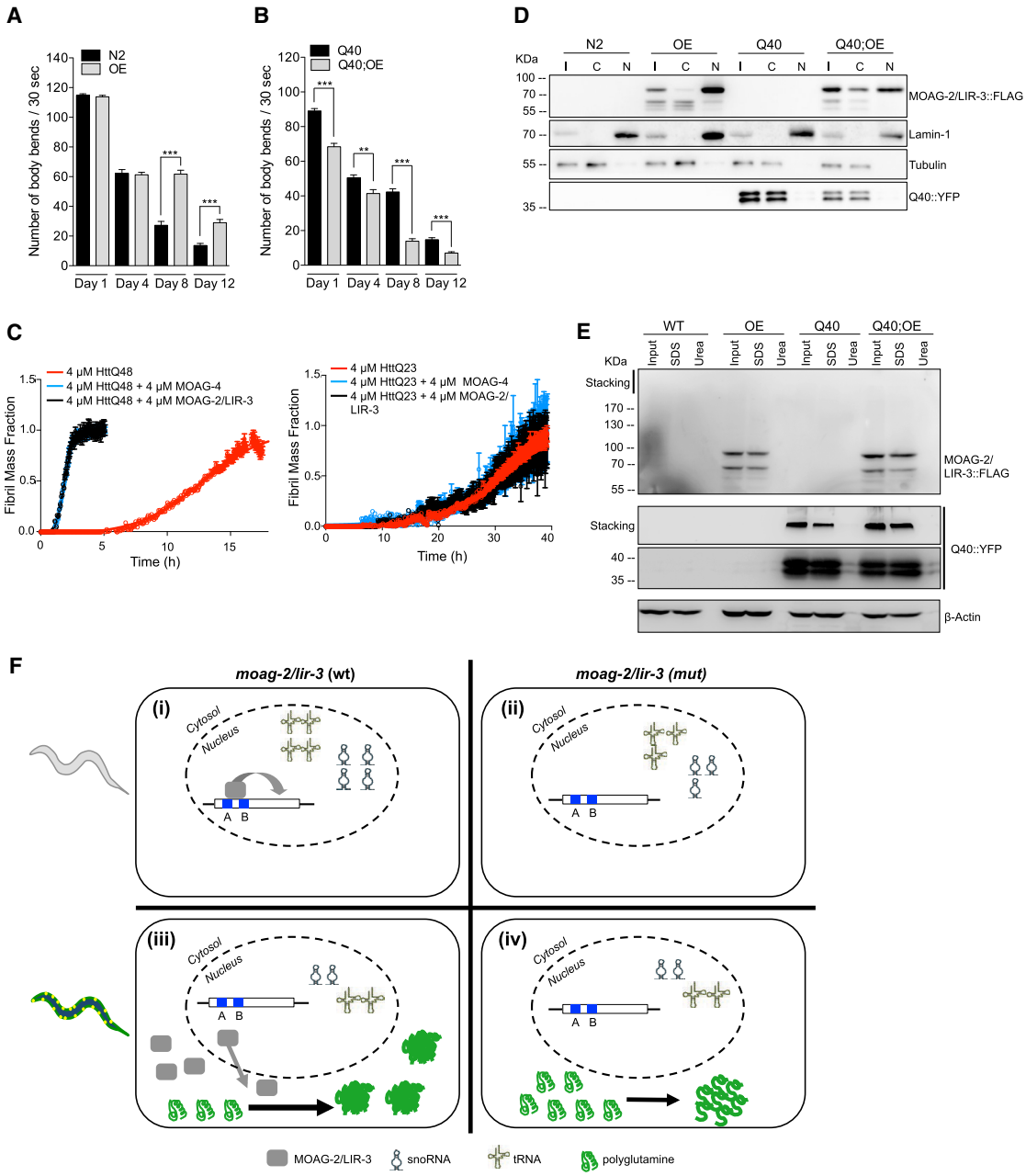

Figure 5. Polyglutamine Moves MOAG-2/LIR-3 Cytosol Where It Turns into a Positive Regulator of Protein Aggregation

(A and B) Number of body bends in N2 wild-type worms and worms overexpressing MOAG-2/LIR-3 (OE) (A) and Q40 wild-type and Q40 worms overexpressing MOAG-2/LIR-3 (Q40;OE) (B). The average of three biological replicates is represented. Data are represented as mean ± SEM and significance was calculated using a two-tailed unpaired Student's t test. **p < 0.01; ***p < 0.001. See also Figure S5A.

(C) Thioflavin T reaction profiles of 4 μM HttQ48 or HttQ23 solutions in the absence or presence of equimolar concentrations of MOAG-2/LIR-3 (black) or the modifier of aggregation MOAG-4 (blue). The concentration of MOAG-2/LIR-3 in whole-organism lysates has been determined to be between 0.3 and 8.5 ppm (http://pax-db.org). The average of four replicates is represented and error bars indicate mean ± SD.

(D) Western blot of subcellular fractionation of MOAG-3/LIR-3, which was detected using α-FLAG antibody. Q40-YFP, LMN-1 (nuclear marker), and α-tubulin (cytosolic marker) were used as controls. See Figure S5C.

(E) Western blot analysis of MOAG-2/LIR-3 SDS solubility from wild-type (WT) and MOAG-2/LIR-3-overexpressing (OE) worms in N2 and polyglutamine worms (Q40). Q40-YFP and β-actin expression were included as controls.

In (D) and (E), the results were generated from L4-stage animals and a representative experiment of three biological replicates is shown.

(F) Model proposing how MOAG-2/LIR-3 drives polyglutamine aggregation. MOAG-2/LIR-3 normally regulates the transcription of small ncRNAs in the nucleus. In the presence of polyglutamine, MOAG-2/LIR-3 is moved to the cytosol, where it exposes an ectopic aggregation-promoting activity.

(HttQ48) with purified MOAG-2/LIR-3 protein and monitored amyloid formation by measuring thioflavin T (ThT) fluorescence in vitro. Our kinetic data revealed that the presence of an equimolar concentration of MOAG-2/LIR-3 accelerated the aggregation of HttQ48, but not of the non-pathogenic form HttQ23, similarly to what was observed in the case of MOAG-4, the *C. elegans* ortholog of SERF1A (Figure 5C). These results indicate that MOAG-2/LIR-3 can catalyze the deposition of aggregation-prone proteins directly.

Polyglutamine Mislocalizes MOAG-2/LIR-3 from the Nucleus to the Cytosol

For a lack of an aggregation-catalyzing effect to explain the reduction of protein aggregation in Q40;*moag-2/lir-3* mutants, MOAG-2/LIR-3 and polyglutamine would, in the wild-type animals, have to localize in the same cellular compartment. Thus, to determine their localization, we performed subcellular fractionations with wild-type and Q40 worms with or without the expression of FLAG-tagged MOAG-2/LIR-3. We found that in the absence of polyglutamine, MOAG-2/LIR-3::FLAG was primarily located in the nucleus (Figure 5D, OE; Figure S5C). Polyglutamine was mostly localized in the cytosol, which was independent of the presence of MOAG-2/LIR-3::FLAG (Figure 5D, Q40 and Q40;OE; Figure S5C). In Q40 worms, however, MOAG-2/LIR-3::FLAG was enriched in the cytosol (Figure 5D, OE and Q40;OE; Figure S5C), which suggests that the presence of polyglutamine altered the localization of MOAG-2/LIR-3. Their joint presence in the cytosol supports a direct interaction between the proteins to drive protein aggregation.

Proteins involved in RNA metabolism have been described to co-aggregate with polyglutamine (Doi et al., 2010; 2008; Schwab et al., 2008), which could explain the retention of MOAG-2/LIR-3 in the cytosol. We therefore fractionated SDS-soluble and insoluble material to determine whether MOAG-2/LIR-3 co-aggregated with polyglutamine. Q40-YFP was detected as low molecular weight monomers and as SDS-resistant species retained in the stacking gel (Figure 5D). The solubility of MOAG-2/LIR-3::FLAG was not altered in the presence of polyglutamine (Figure 5D), suggesting that MOAG-2/LIR-3 is not recruited to SDS-resistant aggregates, but may be associated with the soluble species.

Together, these data suggest that the presence of polyglutamine moves MOAG-2/LIR-3 from the nucleus to the cytosol, where it turns into a positive regulator of protein aggregation, which is at the expense of its function as a transcriptional regulator (Figure 5F).

DISCUSSION

From a genetic screen in a *C. elegans* model of protein aggregation disease, we identified MOAG-2/LIR-3 as a regulator of Pol III transcription in the nucleus and showed that—in the presence of polyglutamine—this protein switches into a positive regulator of polyglutamine aggregation in the cytosol.

Our finding that MOAG-2/LIR-3 is a regulator of transcription confirms predictions about the function of the lir-3 gene. Its role as a transcriptional regulator has been suggested on the basis of its structural similarity to the C2H2 zinc fingers of LIN-26, a fate regulator responsible for the differentiation of non-neuronal ectodermal cells and somatic gonad epithelium (den Boer et al., 1998; Dufourcq et al., 1999; Labouesse et al., 1996). We showed that MOAG-2/LIR-3 is required for the transcription of snRNA, snoRNA, and tRNA genes. In addition, we also showed that unlike other transcription factors that have on occasion been found to bind to the promoters of small ncRNAs, MOAG-2/LIR-3 is associated with the same target genes as the Pol III complex (Niu et al., 2011).

MOAG-2/LIR-3 is known to be expressed in the nuclei of a subset of cell types of *C. elegans*, namely body wall muscle cells, the vulval muscles, the spermatheca, the head and tail ganglia, and the ventral nerve cord, from embryogenesis throughout adulthood (https://transgeneome.mpi-cbg.de/transgeneomics/index.html, March 2014; Reece-Hoyes et al., 2005, 2007). A microarray performed in two distinct mechanosensory neurons—the touch receptor neurons and the FLP neurons—revealed that *moag-2/lir-3* is upregulated in the FLP sensory neurons, suggesting that *moag-2/lir-3* is required for FLP differentiation (Topalidou and Chalfie, 2011). The observation that the expression of MOAG-2/LIR-3 is limited to a subset of cell types suggests that this protein could be a tissue-specific regulator of transcription rather than a core component of the Pol III machinery. Such cell-type-specific regulators of Pol III have been described for human cells and proposed to accommodate cell-specific needs for small ncRNAs (Alla and Cairns, 2014; Oler et al., 2010; also reviewed in Marshall and White, 2008; White, 2011). Whether MOAG-2/LIR-3 has a similar role remains to be established, but it could explain why mutations in the *moag-2/lir-3* gene do not result in any obvious abnormalities in terms of growth or viability.

In *C. elegans*, the nuclear pore protein NPP-13 has been described to associate with the Pol III complex, which regulates the efficient processing of snoRNA and tRNA transcripts (Ikegami and Lieb, 2013). Knockdown of NPP-13 results in abnormally long snoRNA and tRNA transcripts that cannot be processed into their mature form (Ikegami and Lieb, 2013). In *moag-2/lir-3* mutant worms, we did not find unprocessed transcripts for snoRNA or for tRNAs (data not shown), which excludes the possibility that MOAG-2/LIR-3 is required for Pol III transcript processing. Moreover, knockdown of NPP-13 did not alter aggregation, which suggests that mutations in *moag-2/lir-3* do not alter aggregation by interfering with the nuclear pore complex.

Polyglutamine proteins can undergo post-translational modifications, including acetylation, phosphorylation, ubiquitation, and sumoylation (reviewed in Ehrnhoefer et al., 2011; Pennuto et al., 2009). These post-translational modifications have been shown to modulate polyglutamine toxicity and aggregation (Gu et al., 2009; Jana et al., 2005; Matsumoto et al., 2004; Steffan et al., 2004; Thomas et al., 2004). One possibility that could explain the reduction of aggregation observed in the polyglutamine model is that mutations in *moag-2/lir-3* alter the post-translational status of polyglutamine. Although with our present results we cannot exclude this possibility, our in vitro data (Figure 5C) show that MOAG-2/LIR-3 is able to drive polyglutamine aggregation directly in conditions where post-translational modifications do not occur, supporting a functional interaction between MOAG-2/LIR-3 and polyglutamine.

In this study, expression of polyglutamine downregulated the levels of snRNAs, snoRNAs, and tRNAs, demonstrating that aggregation-prone proteins can affect small ncRNA homeostasis. A possible explanation for this downregulation is that the aggregation-prone proteins blocked the nuclear localization of MOAG-2/LIR-3 and perhaps also components of the Pol III complex. Indeed, our data suggest that polyglutamine retains MOAG-2/LIR-3 in the cytosol, which is consistent with the recent finding that aggregation-prone proteins block trafficking in and out of the nucleus (Woerner et al., 2016). Several intrinsically disordered proteins—which include proteins involved in transcriptional regulation—are known to be sequestered by aggregation-prone proteins (Iakoucheva et al., 2002; Liu et al., 2006; Minezaki et al., 2006; Olzscha et al., 2011; Walther et al., 2015). One example is Sp1, which can no longer bind to its DNA targets due to sequestration by mutant *huntingtin* (Dunah et al., 2002; Li et al., 2002). We found that MOAG-2/LIR-3 is not sequestered in the polyglutamine aggregates. The concentration of MOAG-2/LIR-3 in whole-worm lysates has been determined to be between 0.3 and 8.5 ppm (http://pax-db.org). Although these concentrations do not take into account cell- or stage-specific differences in protein expression, its relatively low abundance would support a model in which MOAG-2/LIR-3 drives aggregation via transient interactions with rare SDS-soluble polyglutamine species.

In summary, this work has revealed that protein aggregation can affect the transcription of the non-coding genome by altering the expression of ncRNA genes. Our findings also open up another potential perspective on how aggregation-prone proteins can impair cellular homeostasis: these proteins can convert from their normal functions into aggregation-promoting factors by relocation. These results imply a cellular mechanism whereby aggregation-prone disease-associated proteins inactivate, recruit, and use endogenous proteins that promote their own aggregation and toxicity, which would resemble viral self-catalysis of pathogenesis. We anticipate that interfering with this class of gene products that promote aggregation-prone interactions can be explored for the development of therapies to slow down progression of age-related protein aggregation diseases.

STAR★METHODS

Detailed methods are provided in the online version of this paper and include the following:

- KEY RESOURCES TABLE
- CONTACT FOR REAGENT AND RESOURCE SHARING
- EXPERIMENTAL MODEL AND SUBJECT DETAILS
  - *C. elegans*
- METHOD DETAILS
  - EMS mutagenesis and mapping
  - RNA interference
  - Motility assay
  - Generation of transgenic strains
  - Quantitative PCR
  - Chromatin immunoprecipitation sequencing
  - RNA sequencing
  - Immunofluorescence
  - Filter retardation assay
  - Co-immunoprecipitation
  - Protein insolubility assay
  - Protein purification
  - Aggregation kinetics
  - Subcellular fractionation
  - Bioinformatic analysis
- QUANTIFICATION AND STATISTICAL ANALYSES
  - Quantification of aggregates and motility assay
  - RNA sequencing data analysis
  - Quantitative PCR analysis
  - Filter retardation assay
- DATA AND SOFTWARE AVAILABILITY

SUPPLEMENTAL INFORMATION

Supplemental Information includes five figures and three tables and can be found with this article online at http://dx.doi.org/10.1016/j.molcel.2017.02.022.

AUTHOR CONTRIBUTIONS

O.S. and E.A.A.N. designed the research; O.S. performed most experiments; A.M.-C., M.K., M.A.Z., F.A.A., R.I.S., E.S., C.N.M., H.H.W., W.H., and A.S. participated in the experiments; O.S., T.d.J., R.W.P., E.E.W., M.V., C.F.C., V.R., and V.G. analyzed the data; and O.S. and E.A.A.N. wrote the manuscript with input from all authors.

ACKNOWLEDGMENTS

We thank the Caenorhabditis Genetics Centre (funded by the NIH National Centre for Research Resources and the NIH Office of Research Infrastructure Programs [P40 OD010440]) and the Mitani laboratory for the *C. elegans* strains (funded by the Japan National BioResource Project). We thank Pieter van der Vlies and Jelkje Bergsma for practical assistance with whole-genome sequencing. We thank Pieter Neerincx for help with installing MAQGene. We thank Marianna Bevova and Diana Spierings for assistance with RNA sequencing. We thank Kohta Ikegami for the *npp3* RNAi vector and for the protocols on RNA sequencing and co-immunoprecipitation. We thank the modERN project (NIH U41HG007355) for sharing the MOAG-2/LIR-3 ChIP-seq data prior to publication. We thank Klaas Sjollema for help with *C. elegans* imaging (UMIC, UMCG). We thank Sally Hill for editing this manuscript. This study was supported by funding from the Berlin Institute of Health Collaborative Research Grant no. 1.1.2.a.3 funded by the German Federal Ministry for Education and Research (BMBF) (to E.E.W). This project was funded by a Meervoud Grant from NWO (836.09.001) (to E.A.A.N.), a European Research Council (ERC) starting grant (281622 PDControl) (to E.A.A.N.), the Fundação para a Ciência e Tecnologia fellowship (SFRH/BD/51009/2010) (to O.S.), the Alumni chapter Gooische Groningers facilitated by the Ubbo Emmius Fonds, and a Groningen University Institute for Drug Exploration (GUIDE) fellowship (O.S.).

Received: December 22, 2015
Revised: January 5, 2017
Accepted: February 22, 2017
Published: March 16, 2017

REFERENCES

Alla, R.K., and Cairns, B.R. (2014). RNA polymerase III transcriptomes in human embryonic stem cells and induced pluripotent stem cells, and relationships with pluripotency transcription factors. PLoS ONE *9*, e85648.

Arrasate, M., Mitra, S., Schweitzer, E.S., Segal, M.R., and Finkbeiner, S. (2004). Inclusion body formation reduces levels of mutant huntingtin and the risk of neuronal death. Nature *431*, 805–810.

Bailey, T.L., Bodén, M., Buske, F.A., Frith, M., Grant, C.E., Clementi, L., Ren, J., Li, W.W., and Noble, W.S. (2009). MEME SUITE: tools for motif discovery and searching. Nucleic Acids Res. *37*, W202–W208.

Bigelow, H., Doitsidou, M., Sarin, S., and Hobert, O. (2009). MAQGene: software to facilitate C. elegans mutant genome sequence analysis. Nat. Methods *6*, 549.

Bolognesi, B., Kumita, J.R., Barros, T.P., Esbjorner, E.K., Luheshi, L.M., Crowther, D.C., Wilson, M.R., Dobson, C.M., Favrin, G., and Yerbury, J.J. (2010). ANS binding reveals common features of cytotoxic amyloid species. ACS Chem. Biol. *5*, 735–740.

Bratković, T., and Rogelj, B. (2014). The many faces of small nucleolar RNAs. Biochim. Biophys. Acta *1839*, 438–443.

Brenner, S. (1974). The genetics of Caenorhabditis elegans. Genetics *77*, 71–94.

Brown, R.S. (2005). Zinc finger proteins: getting a grip on RNA. Curr. Opin. Struct. Biol. *15*, 94–98.

Chen, F., Hersh, B.M., Conradt, B., Zhou, Z., Riemer, D., Gruenbaum, Y., and Horvitz, H.R. (2000). Translocation of C. elegans CED-4 to nuclear membranes during programmed cell death. Science *287*, 1485–1489.

Chiti, F., and Dobson, C.M. (2009). Amyloid formation by globular proteins under native conditions. Nat. Chem. Biol. *5*, 15–22.

Davranche, A., Aviolat, H., Zeder-Lutz, G., Busso, D., Altschuh, D., Trottier, Y., and Klein, F.A.C. (2011). Huntingtin affinity for partners is not changed by polyglutamine length: aggregation itself triggers aberrant interactions. Hum. Mol. Genet. *20*, 2795–2806.

den Boer, B.G., Sookhareea, S., Dufourcq, P., and Labouesse, M. (1998). A tissue-specific knock-out strategy reveals that lin-26 is required for the formation of the somatic gonad epithelium in Caenorhabditis elegans. Development *125*, 3213–3224.

Doi, H., Okamura, K., Bauer, P.O., Furukawa, Y., Shimizu, H., Kurosawa, M., Machida, Y., Miyazaki, H., Mitsui, K., Kuroiwa, Y., and Nukina, N. (2008). RNA-binding protein TLS is a major nuclear aggregate-interacting protein in huntingtin exon 1 with expanded polyglutamine-expressing cells. J. Biol. Chem. *283*, 6489–6500.

Doi, H., Koyano, S., Suzuki, Y., Nukina, N., and Kuroiwa, Y. (2010). The RNA-binding protein FUS/TLS is a common aggregate-interacting protein in polyglutamine diseases. Neurosci. Res. *66*, 131–133.

Duerr, J.S. (2006). Immunohistochemistry. In WormBook (WormBook), pp. 1–61.

Dufourcq, P., Chanal, P., Vicaire, S., Camut, E., Quintin, S., den Boer, B.G., Bosher, J.M., and Labouesse, M. (1999). lir-2, lir-1 and lin-26 encode a new class of zinc-finger proteins and are organized in two overlapping operons both in Caenorhabditis elegans and in Caenorhabditis briggsae. Genetics *152*, 221–235.

Dunah, A.W., Jeong, H., Griffin, A., Kim, Y.-M., Standaert, D.G., Hersch, S.M., Mouradian, M.M., Young, A.B., Tanese, N., and Krainc, D. (2002). Sp1 and TAFII130 transcriptional activity disrupted in early Huntington's disease. Science *296*, 2238–2243.

Ehrnhoefer, D.E., Sutton, L., and Hayden, M.R. (2011). Small changes, big impact: posttranslational modifications and function of huntingtin in Huntington disease. Neuroscientist *17*, 475–492.

Eisenberg, D., and Jucker, M. (2012). The amyloid state of proteins in human diseases. Cell *148*, 1188–1203.

Falsone, S.F., Meyer, N.H., Schrank, E., Leitinger, G., Pham, C.L.L., Fodero-Tavoletti, M.T., Holmberg, M., Dulle, M., Scicluna, B., Gesslbauer, B., et al. (2012). SERF protein is a direct modifier of amyloid fiber assembly. Cell Rep. *2*, 358–371.

Garcia, S.M., Casanueva, M.O., Silva, M.C., Amaral, M.D., and Morimoto, R.I. (2007). Neuronal signaling modulates protein homeostasis in Caenorhabditis elegans post-synaptic muscle cells. Genes Dev. *21*, 3006–3016.

Gerstein, M.B., Lu, Z.J., Van Nostrand, E.L., Cheng, C., Arshinoff, B.I., Liu, T., Yip, K.Y., Robilotto, R., Rechtsteiner, A., Ikegami, K., et al.; modENCODE Consortium (2010). Integrative analysis of the Caenorhabditis elegans genome by the modENCODE project. Science *330*, 1775–1787.

Gidalevitz, T., Ben-Zvi, A., Ho, K.H., Brignull, H.R., and Morimoto, R.I. (2006). Progressive disruption of cellular protein folding in models of polyglutamine diseases. Science *311*, 1471–1474.

Gu, X., Greiner, E.R., Mishra, R., Kodali, R., Osmand, A., Finkbeiner, S., Steffan, J.S., Thompson, L.M., Wetzel, R., and Yang, X.W. (2009). Serines 13 and 16 are critical determinants of full-length human mutant huntingtin induced disease pathogenesis in HD mice. Neuron *64*, 828–840.

Guthrie, C., and Patterson, B. (1988). Spliceosomal snRNAs. Annu. Rev. Genet. *22*, 387–419.

Hall, T.M.T. (2005). Multiple modes of RNA recognition by zinc finger proteins. Curr. Opin. Struct. Biol. *15*, 367–373.

Hamamichi, S., Rivas, R.N., Knight, A.L., Cao, S., Caldwell, K.A., and Caldwell, G.A. (2008). Hypothesis-based RNAi screening identifies neuroprotective genes in a Parkinson's disease model. Proc. Natl. Acad. Sci. USA *105*, 728–733.

Hsu, A.-L., Murphy, C.T., and Kenyon, C. (2003). Regulation of aging and age-related disease by DAF-16 and heat-shock factor. Science *300*, 1142–1145.

Iakoucheva, L.M., Brown, C.J., Lawson, J.D., Obradović, Z., and Dunker, A.K. (2002). Intrinsic disorder in cell-signaling and cancer-associated proteins. J. Mol. Biol. *323*, 573–584.

Ikegami, K., and Lieb, J.D. (2013). Integral nuclear pore proteins bind to Pol III-transcribed genes and are required for Pol III transcript processing in C. elegans. Mol. Cell *51*, 840–849.

Ikegami, K., Egelhofer, T.A., Strome, S., and Lieb, J.D. (2010). Caenorhabditis elegans chromosome arms are anchored to the nuclear membrane via discontinuous association with LEM-2. Genome Biol. *11*, R120.

Jana, N.R., Dikshit, P., Goswami, A., Kotliarova, S., Murata, S., Tanaka, K., and Nukina, N. (2005). Co-chaperone CHIP associates with expanded polyglutamine protein and promotes their degradation by proteasomes. J. Biol. Chem. *280*, 11635–11640.

Jorgensen, E.M., and Mango, S.E. (2002). The art and design of genetic screens: caenorhabditis elegans. Nat. Rev. Genet. *3*, 356–369.

Kasper, D.M., Wang, G., Gardner, K.E., Johnstone, T.G., and Reinke, V. (2014). The C. elegans SNAPc component SNPC-4 coats piRNA domains and is globally required for piRNA abundance. Dev. Cell *31*, 145–158.

Kayed, R., Head, E., Thompson, J.L., McIntire, T.M., Milton, S.C., Cotman, C.W., and Glabe, C.G. (2003). Common structure of soluble amyloid oligomers implies common mechanism of pathogenesis. Science *300*, 486–489.

Kim, D., Pertea, G., Trapnell, C., Pimentel, H., Kelley, R., and Salzberg, S.L. (2013). TopHat2: accurate alignment of transcriptomes in the presence of insertions, deletions and gene fusions. Genome Biol. *14*, R36.

Kosugi, S., Hasebe, M., Tomita, M., and Yanagawa, H. (2009). Systematic identification of cell cycle-dependent yeast nucleocytoplasmic shuttling proteins by prediction of composite motifs. Proc. Natl. Acad. Sci. USA *106*, 10171–10176.

Krishna, S.S., Majumdar, I., and Grishin, N.V. (2003). Structural classification of zinc fingers: survey and summary. Nucleic Acids Res. *31*, 532–550.

Kuwahara, T., Koyama, A., Koyama, S., Yoshina, S., Ren, C.-H., Kato, T., Mitani, S., and Iwatsubo, T. (2008). A systematic RNAi screen reveals involvement of endocytic pathway in neuronal dysfunction in alpha-synuclein transgenic C. elegans. Hum. Mol. Genet. *17*, 2997–3009.

Labouesse, M., Hartwieg, E., and Horvitz, H.R. (1996). The Caenorhabditis elegans LIN-26 protein is required to specify and/or maintain all non-neuronal ectodermal cell fates. Development *122*, 2579–2588.

Lee, V.M., Wang, J., and Trojanowski, J.Q. (1999). Purification of paired helical filament tau and normal tau from human brain tissue. Methods Enzymol. *309*, 81–89.

Lejeune, F.-X., Mesrob, L., Parmentier, F., Bicep, C., Vazquez-Manrique, R.P., Parker, J.A., Vert, J.-P., Tourette, C., and Néri, C. (2012). Large-scale functional

RNAi screen in C. elegans identifies genes that regulate the dysfunction of mutant polyglutamine neurons. BMC Genomics *13*, 91.

Letunic, I., Doerks, T., and Bork, P. (2012). SMART 7: recent updates to the protein domain annotation resource. Nucleic Acids Res. *40*, D302–D305.

Li, S.-H., Cheng, A.L., Zhou, H., Lam, S., Rao, M., Li, H., and Li, X.-J. (2002). Interaction of Huntington disease protein with transcriptional activator Sp1. Mol. Cell. Biol. *22*, 1277–1287.

Liu, J., Perumal, N.B., Oldfield, C.J., Su, E.W., Uversky, V.N., and Dunker, A.K. (2006). Intrinsic disorder in transcription factors. Biochemistry *45*, 6873–6888.

Livak, K.J., and Schmittgen, T.D. (2001). Analysis of relative gene expression data using real-time quantitative PCR and the 2(-Delta Delta C(T)) method. Methods *25*, 402–408.

Marshall, L., and White, R.J. (2008). Non-coding RNA production by RNA polymerase III is implicated in cancer. Nat. Rev. Cancer *8*, 911–914.

Matsumoto, M., Yada, M., Hatakeyama, S., Ishimoto, H., Tanimura, T., Tsuji, S., Kakizuka, A., Kitagawa, M., and Nakayama, K.I. (2004). Molecular clearance of ataxin-3 is regulated by a mammalian E4. EMBO J. *23*, 659–669.

McCarthy, D.J., Chen, Y., and Smyth, G.K. (2012). Differential expression analysis of multifactor RNA-seq experiments with respect to biological variation. Nucleic Acids Res. *40*, 4288–4297.

Miller, J., Arrasate, M., Brooks, E., Libeu, C.P., Legleiter, J., Hatters, D., Curtis, J., Cheung, K., Krishnan, P., Mitra, S., et al. (2011). Identifying polyglutamine protein species in situ that best predict neurodegeneration. Nat. Chem. Biol. *7*, 925–934.

Minezaki, Y., Homma, K., Kinjo, A.R., and Nishikawa, K. (2006). Human transcription factors contain a high fraction of intrinsically disordered regions essential for transcriptional regulation. J. Mol. Biol. *359*, 1137–1149.

Nillegoda, N.B., Kirstein, J., Szlachcic, A., Berynskyy, M., Stank, A., Stengel, F., Arnsburg, K., Gao, X., Scior, A., Aebersold, R., et al. (2015). Crucial HSP70 co-chaperone complex unlocks metazoan protein disaggregation. Nature *524*, 247–251.

Niu, W., Lu, Z.J., Zhong, M., Sarov, M., Murray, J.I., Brdlik, C.M., Janette, J., Chen, C., Alves, P., Preston, E., et al. (2011). Diverse transcription factor binding features revealed by genome-wide ChIP-seq in C. elegans. Genome Res. *21*, 245–254.

Nollen, E.A.A., Garcia, S.M., van Haaften, G., Kim, S., Chavez, A., Morimoto, R.I., and Plasterk, R.H.A. (2004). Genome-wide RNA interference screen identifies previously undescribed regulators of polyglutamine aggregation. Proc. Natl. Acad. Sci. USA *101*, 6403–6408.

Notredame, C., Higgins, D.G., and Heringa, J. (2000). T-Coffee: a novel method for fast and accurate multiple sequence alignment. J. Mol. Biol. *302*, 205–217.

Oler, A.J., Alla, R.K., Roberts, D.N., Wong, A., Hollenhorst, P.C., Chandler, K.J., Cassiday, P.A., Nelson, C.A., Hagedorn, C.H., Graves, B.J., and Cairns, B.R. (2010). Human RNA polymerase III transcriptomes and relationships to Pol II promoter chromatin and enhancer-binding factors. Nat. Struct. Mol. Biol. *17*, 620–628.

Olzscha, H., Schermann, S.M., Woerner, A.C., Pinkert, S., Hecht, M.H., Tartaglia, G.G., Vendruscolo, M., Hayer-Hartl, M., Hartl, F.U., and Vabulas, R.M. (2011). Amyloid-like aggregates sequester numerous metastable proteins with essential cellular functions. Cell *144*, 67–78.

Pennuto, M., Palazzolo, I., and Poletti, A. (2009). Post-translational modifications of expanded polyglutamine proteins: impact on neurotoxicity. Hum. Mol. Genet. *18* (R1), R40–R47.

Prilusky, J., Felder, C.E., Zeev-Ben-Mordehai, T., Rydberg, E.H., Man, O., Beckmann, J.S., Silman, I., and Sussman, J.L. (2005). FoldIndex: a simple tool to predict whether a given protein sequence is intrinsically unfolded. Bioinformatics *21*, 3435–3438.

Rampelt, H., Kirstein-Miles, J., Nillegoda, N.B., Chi, K., Scholz, S.R., Morimoto, R.I., and Bukau, B. (2012). Metazoan Hsp70 machines use Hsp110 to power protein disaggregation. EMBO J. *31*, 4221–4235.

Reece-Hoyes, J.S., Deplancke, B., Shingles, J., Grove, C.A., Hope, I.A., and Walhout, A.J.M. (2005). A compendium of Caenorhabditis elegans regulatory transcription factors: a resource for mapping transcription regulatory networks. Genome Biol. *6*, R110.

Reece-Hoyes, J.S., Shingles, J., Dupuy, D., Grove, C.A., Walhout, A.J.M., Vidal, M., and Hope, I.A. (2007). Insight into transcription factor gene duplication from Caenorhabditis elegans Promoterome-driven expression patterns. BMC Genomics *8*, 27.

Robinson, M.D., McCarthy, D.J., and Smyth, G.K. (2010). edgeR: a Bioconductor package for differential expression analysis of digital gene expression data. Bioinformatics *26*, 139–140.

Sarov, M., Murray, J.I., Schanze, K., Pozniakovski, A., Niu, W., Angermann, K., Hasse, S., Rupprecht, M., Vinis, E., Tinney, M., et al. (2012). A genome-scale resource for in vivo tag-based protein function exploration in C. elegans. Cell *150*, 855–866.

Scherzinger, E., Lurz, R., Turmaine, M., Mangiarini, L., Hollenbach, B., Hasenbank, R., Bates, G.P., Davies, S.W., Lehrach, H., and Wanker, E.E. (1997). Huntingtin-encoded polyglutamine expansions form amyloid-like protein aggregates in vitro and in vivo. Cell *90*, 549–558.

Schramm, L., and Hernandez, N. (2002). Recruitment of RNA polymerase III to its target promoters. Genes Dev. *16*, 2593–2620.

Schultz, J., Milpetz, F., Bork, P., and Ponting, C.P. (1998). SMART, a simple modular architecture research tool: identification of signaling domains. Proc. Natl. Acad. Sci. USA *95*, 5857–5864.

Schwab, C., Arai, T., Hasegawa, M., Yu, S., and McGeer, P.L. (2008). Colocalization of transactivation-responsive DNA-binding protein 43 and huntingtin in inclusions of Huntington disease. J. Neuropathol. Exp. Neurol. *67*, 1159–1165.

Shankar, G.M., Li, S., Mehta, T.H., Garcia-Munoz, A., Shepardson, N.E., Smith, I., Brett, F.M., Farrell, M.A., Rowan, M.J., Lemere, C.A., et al. (2008). Amyloid-beta protein dimers isolated directly from Alzheimer's brains impair synaptic plasticity and memory. Nat. Med. *14*, 837–842.

Silva, M.C., Fox, S., Beam, M., Thakkar, H., Amaral, M.D., and Morimoto, R.I. (2011). A genetic screening strategy identifies novel regulators of the proteostasis network. PLoS Genet. *7*, e1002438.

Sin, O., and Nollen, E.A.A. (2015). Regulation of protein homeostasis in neurodegenerative diseases: the role of coding and non-coding genes. Cell. Mol. Life Sci. *72*, 4027–4047.

Sittler, A., Wälter, S., Wedemeyer, N., Hasenbank, R., Scherzinger, E., Eickhoff, H., Bates, G.P., Lehrach, H., and Wanker, E.E. (1998). SH3GL3 associates with the Huntingtin exon 1 protein and promotes the formation of polygln-containing protein aggregates. Mol. Cell *2*, 427–436.

Soto, C. (2003). Unfolding the role of protein misfolding in neurodegenerative diseases. Nat. Rev. Neurosci. *4*, 49–60.

Steffan, J.S., Agrawal, N., Pallos, J., Rockabrand, E., Trotman, L.C., Slepko, N., Illes, K., Lukacsovich, T., Zhu, Y.-Z., Cattaneo, E., et al. (2004). SUMO modification of Huntingtin and Huntington's disease pathology. Science *304*, 100–104.

Thomas, M., Dadgar, N., Aphale, A., Harrell, J.M., Kunkel, R., Pratt, W.B., and Lieberman, A.P. (2004). Androgen receptor acetylation site mutations cause trafficking defects, misfolding, and aggregation similar to expanded glutamine tracts. J. Biol. Chem. *279*, 8389–8395.

Topalidou, I., and Chalfie, M. (2011). Shared gene expression in distinct neurons expressing common selector genes. Proc. Natl. Acad. Sci. USA *108*, 19258–19263.

van der Goot, A.T., Zhu, W., Vázquez-Manrique, R.P., Seinstra, R.I., Dettmer, K., Michels, H., Farina, F., Krijnen, J., Melki, R., Buijsman, R.C., et al. (2012). Delaying aging and the aging-associated decline in protein homeostasis by inhibition of tryptophan degradation. Proc. Natl. Acad. Sci. USA *109*, 14912–14917.

van Ham, T.J., Holmberg, M.A., van der Goot, A.T., Teuling, E., Garcia-Arencibia, M., Kim, H.-E., Du, D., Thijssen, K.L., Wiersma, M., Burggraaff, R., et al. (2010). Identification of MOAG-4/SERF as a regulator of age-related proteotoxicity. Cell *142*, 601–612.

Walther, D.M., Kasturi, P., Zheng, M., Pinkert, S., Vecchi, G., Ciryam, P., Morimoto, R.I., Dobson, C.M., Vendruscolo, M., Mann, M., and Hartl, F.U. (2015). Widespread proteome remodeling and aggregation in aging C. elegans. Cell *161*, 919–932.

Wanker, E.E., Scherzinger, E., Heiser, V., Sittler, A., Eickhoff, H., and Lehrach, H. (1999). Membrane filter assay for detection of amyloid-like polyglutamine-containing protein aggregates. Methods Enzymol. *309*, 375–386.

White, R.J. (2011). Transcription by RNA polymerase III: more complex than we thought. Nat. Rev. Genet. *12*, 459–463.

Wicks, S.R., Yeh, R.T., Gish, W.R., Waterston, R.H., and Plasterk, R.H. (2001). Rapid gene mapping in Caenorhabditis elegans using a high density polymorphism map. Nat. Genet. *28*, 160–164.

Woerner, A.C., Frottin, F., Hornburg, D., Feng, L.R., Meissner, F., Patra, M., Tatzelt, J., Mann, M., Winklhofer, K.F., Hartl, F.U., and Hipp, M.S. (2016). Cytoplasmic protein aggregates interfere with nucleocytoplasmic transport of protein and RNA. Science *351*, 173–176.

Yanamandra, K., Jiang, H., Mahan, T.E., Maloney, S.E., Wozniak, D.F., Diamond, M.I., and Holtzman, D.M. (2015). Anti-tau antibody reduces insoluble tau and decreases brain atrophy. Ann. Clin. Transl. Neurol. *2*, 278–288.

Zhong, M., Niu, W., Lu, Z.J., Sarov, M., Murray, J.I., Janette, J., Raha, D., Sheaffer, K.L., Lam, H.Y.K., Preston, E., et al. (2010). Genome-wide identification of binding sites defines distinct functions for Caenorhabditis elegans PHA-4/FOXA in development and environmental response. PLoS Genet. *6*, e1000848.

STAR★METHODS

KEY RESOURCES TABLE

REAGENT or RESOURCE	SOURCE	IDENTIFIER
Antibodies		
Goat anti-GFP for ChIP-seq experiment	gift from Kevin White	N/A
Mouse anti-FLAG M2	Sigma-Aldrich	Cat# F3165, RRID: AB_259529
Mouse anti-GFP	Clontech Laboratories	Cat# 632381, RRID: AB_2313808
Mouse α-tubulin	Sigma-Aldrich	Cat# T6074, RRID: AB_477582
Goat anti-mouse Cyanine 5	Thermo Fisher	Cat# A10524, RRID: AB_2534033
Rabbit anti-Pol II (ama-1 subunit)	Novus Biologicals	Cat# 38520002, RRID: AB_10709680
Rabbit anti-Pol III (rpc-1 subunit)	Novus Biologicals	Cat# 5333.00.02, RRID: AB_2616364
Rabbit anti-LMN-1	Novus Biologicals	Cat# 38530002, RRID: AB_10005072
Chemicals, Peptides, and Recombinant Proteins		
Trizol	Life Technologies	Cat#15596-018
Vectashield Mounting Medium (DAPI)	Vector Labs	Cat#H-1200
Critical Commercial Assays		
ECL Prime Western Blotting Detection Reagent	Amersham	Cat#RPN2232
RevertAid H Minus First Strand cDNA Synthesis kit	Life Technologies	Cat#K1632
SYBR Green Dye	Bio-Rad	Cat#172-5125
Qubit RNA HS Assay Kit	Thermo Fisher	Cat#Q32852
TruSeq Sample Preparation V2 Kit	Illumina	RS-122-2001, RS-122-2002
Ribominus Eukaryote Kit	Invitrogen	Cat#A10837-08
Fragmentation Buffer	Ambion	Cat#AM8740
DNase I	Fermentas	Cat#EN0521
Deposited Data		
ChIP-seq data	ENCODE	ENCODE: ENCSR408FDZ
ChIP-seq data	ArrayExpress	ArrayExpress: E-MTAB-4174
RNA-seq data	ArrayExpress	ArrayExpress: E-MTAB-4172
Mendeley Data	This paper	http://dx.doi.org/10.17632/knzkvgbf6x.2
Experimental Models: Organisms/Strains		
C. elegans strains are listed in Table S1.	N/A	N/A
Oligonucleotides		
Primer F1: CGCTCACAGTCAACGTCG	This paper	N/A
Primer R1: CCATGCGATTTGACACATTTCG	This paper	N/A
Primer F2: CGGCATTGCTCTTGTCGTGC	This paper	N/A
Primer R2: GCATCTCATGAAACCAGACGC	This paper	N/A
cdc-42_F3: TGAAAGCAGTGAAATACG TTGAA	This paper	N/A
cdc-42_R3: TGTTGTGGTGGGTCGAGAG	This paper	N/A
lir-3_F4: TTCTCCATATCCAGTGCATGA	This paper	N/A
lir-3_R4: TGAAGCTTCCTGTCGGATG	This paper	N/A
rpc-1_F1: GGAAGCCTATAAAACATCACTTC	This paper	N/A
rpc1_R1: GAGTCGATGGTTCTCCAAT ACTAG	This paper	N/A
rps-21_F1: CGTTCCACGCAAGTGCTCTTCG	This paper	N/A
rps-21_R1: CTTTCCTGGGATCATGCGGCC	This paper	N/A

(*Continued on next page*)

Continued

REAGENT or RESOURCE	SOURCE	IDENTIFIER
Recombinant DNA		
pGEM-T Easy Vector	Promega	Cat#A1380
pPD136.61 [P(unc-54)::CFP]	Addgene	Cat#1682
pENG603 [P(lir-3)::lir-3]	This paper	N/A
Software and Algorithms		
CLC Bio	www.clcbio.com	N/A
MAQGene	Bigelow et al., 2009	http://maqweb.sourceforge.net/
Leica Application Suite X	Leica	N/A
TopHat 2.0.9	Kim et al., 2013	http://ccb.jhu.edu/software/tophat/index.shtml
EdgeR	Robinson et al., 2010; McCarthy et al., 2012	http://bioconductor.org
ImageJ	Open source	N/A
SMART	Letunic et al., 2012; Schultz et al., 1998	http://smart.embl-heidelberg.de/
NLS Mapper	Kosugi et al., 2009	http://nls-mapper.iab.keio.ac.jp/cgi-bin/NLS_Mapper_form.cgi
FoldIndex	Prilusky et al., 2005	http://bioportal.weizmann.ac.il/fldbin/findex
MEME Suite	Bailey et al., 2009	http://meme-suite.org/
BLAST	Open source	https://blast.ncbi.nlm.nih.gov/Blast.cgi
T-Coffee	Notredame et al., 2000	http://www.ebi.ac.uk/Tools/msa/tcoffee/
ORF Finder	Open source	https://www.ncbi.nlm.nih.gov/gorf/orfig.cgi
Other		
Confocal laser scanning microscope: TCS SP8	Leica	N/A
FastPrep 24 Instrument	MP Biomedicals	Cat#116004500
48-well Bio-Dot microfiltration system	Bio-Rad	Cat#1703938
HiSeq 2500 Instrument	Illumina	N/A

CONTACT FOR REAGENT AND RESOURCE SHARING

Further information and requests for resources and reagents should be directed to and will be fulfilled by the Lead Contact, Ellen A.A. Nollen (e.a.a.nollen@umcg.nl). Published research materials and reagents from the ERIBA are shared with the academic community under a Material Transfer Agreement (MTA).

EXPERIMENTAL MODEL AND SUBJECT DETAILS

C. elegans

The strains used in this study are listed in Table S1. Standard methods were used for culturing *C. elegans* at 20°C (Brenner, 1974). The LIR-3 overexpression strain (OP312) was generated by biolistic transformation to produce an integrated, low-copy transgene of the WRM0637aB05 fosmid, recombined with GFP::3xFLAG in frame at the carboxy terminus of the *lir-3* locus (Sarov et al., 2012). To synchronize animals, eggs were collected from gravid hermaphrodites by hypochlorite bleaching and hatched overnight in M9 buffer. The desired numbers of L1 animals were subsequently cultured on nematode growth medium (NGM) agar plates seeded with OP50 bacteria.

METHOD DETAILS

EMS mutagenesis and mapping

Mutagenesis was performed using standard *C. elegans* ethyl methanesulfonate (EMS) methodology (Jorgensen and Mango, 2002). 8000 mutagenized genomes were screened for suppressors of aggregation. *moag-2(pk2183)* was identified by single-nucleotide polymorphism mapping to a region between base 9,400,743 and 11,827,697 on linkage group II (Wicks et al., 2001). Next generation sequencing was performed in that region to identify candidate genes for *moag-2*. CLC Bio and MAQGene software were utilized for mapping the mutation in F37H8.1 (listed in Key Resources Table).

RNA interference

RNAi experiments were performed on NGM agar plates containing 1 mM IPTG and 50 mg/ml ampicillin and seeded with RNAi bacteria induced with IPTG to produce dsRNA. Worms were synchronized by hypochlorite bleaching; L1 worms were grown on RNAi plates and used for the experiments at L4 stage, unless stated otherwise. Plates were coded so that the experimenter was blind to the genotype of the animal.

Motility assay

At day 1, 4, 8 and 12 of adulthood, animals were placed in a drop of M9 and were allowed to recover for 30 s after which the number of body bends was counted for 30 s. Fifteen animals were counted per experiment and the data from three biological replicates was combined. Plates were coded so that the experimenter was blind to the genotype of the animal. The experiments with the N2 worms and the Q40 animals were performed independently due to growth differences between the strains. In our laboratory conditions, N2 worms take approximately 72 hr to reach L4 stage after hypochlorite treatment, whereas Q40 take approximately 96 hr.

Generation of transgenic strains

For the rescue experiment, a genomic construct of *lir-3* spanning 1500 bp upstream to 330 bp downstream of F37H8.1 was amplified from N2 genomic DNA by nested PCR using primers F1; R1; F2 and R2 (primer sequences listed in the Key Resources Table). The resulting PCR fragment was cloned into the pGEM-T Easy Vector (#A1380, Promega) and sequenced. Transgenic lines were made by injecting ~20 ng/μl of construct along with ~10 ng/μl of pPD136.61 [P(*unc-54::CFP*)] into N2 animals. Two independent lines were obtained for each transgene of interest.

Quantitative PCR

Total RNA was extracted from synchronized populations in L4 stage using Trizol (#15596-018, Life Technologies) according to the manufacturer's description. Total RNA quality and concentration were assessed using a NanoDrop 2000 spectrophotometer (Thermo Scientific). cDNA was made from 2 μg total *C. elegans* RNA with a RevertAid H Minus First Strand cDNA Synthesis kit (#K1632, Life Technologies) using random hexamer primers. Quantitative real-time PCR was performed using a Roche LightCycler 480 Instrument II (Roche Diagnostics) with SYBR green dye (#172-5125, Bio-Rad) to detect DNA amplification. The following cycle conditions were used: 50°C for 10 min, 95°C for 10 min, followed by 40 cycles at 95°C for 15 s and 57°C for 30 s. Relative transcript levels were quantitated using a standard curve of pooled cDNA solutions. Expression levels were normalized against the endogenous reference gene *cdc-42*. The following primers were used: cdc-42_F3; cdc-42_R3; lir-3_F4 and lir-3_R4 (primer sequences listed in the Key Resources Table).

To measure the efficiency of Pol III knockdown by RNAi, total RNA from 20 L4 animals was extracted using Trizol (Life Technologies). As a quality control step, total RNA was measured using Qubit RNA HS Assay Kit (#Q32852, Thermo Fisher). Following DNase I digestion (#EN0521, Fermentas), total RNA was purified with Trizol (Life Technologies). First strand synthesis was carried out using Superscript II (Invitrogen) using random hexamer primers. Expression levels were normalized to the expression of *rps-21* following the $2^{-\Delta\Delta CT}$ method (Livak and Schmittgen, 2001). The primers used were rpc-1_F1; rpc1_R1; rps-21_F1 and rps-21_R1 (primer sequences listed in the Key Resources Table).

Chromatin immunoprecipitation sequencing

ChIP assays were conducted as previously described (Niu et al., 2011; Zhong et al., 2010). Worm staging was achieved by bleaching and L1 starvation. Arrested L1 worms were plated on peptone-enriched NGM plates seeded with OP50 bacteria and grown for 48 hr for L4 collection at 20°C. Samples were cross-linked with 2% formaldehyde for 30 min at room temperature and then quenched with 1 M Tris pH 7.5. The pelleted worms were subsequently flash frozen in liquid nitrogen and stored at −80°C. Samples were sonicated using a microtip to obtain DNA fragments mostly 200 to 800 bp in length. For each sample, 2.2 or 4.4 mg of cell extract was immunoprecipitated using a goat α-GFP antibody, GoatV (gift from Kevin White).

For library preparation and sequencing we used the enriched DNA fragments and input control (genomic DNA from the same sample) for two biological replicates as previously described (Kasper et al., 2014). Briefly, samples were multiplexed using the Ovation Ultralow DR Multiplex Systems 1-8 and 9-16 (NuGEN Technologies) following the manufacturer's protocol, with the exception that QIAGEN MinElute PCR purification kits were used to isolate the DNA. Library size selection in the 200-800 bp range was achieved using the SPRIselect reagent kit (Beckman Coulter) and sequencing was performed on the Illumina HiSeq 2000 platform. To search for MOAG-2/LIR-3-specific binding sites, we only considered binding sites consistent across both replicates and within a range of −400 bp to +100 bp relative to the TSS. In addition, to avoid false positives in our analysis we excluded highly occupied target regions (Gerstein et al., 2010). The ChIP seq data used was obtained from modENCODE DCC (http://www.modencode.org, September 2014). All ChIP seq data were deposited in the ENCODE database, under ID code ENCSR408FDZ and in ArrayExpress, under accession number E-MTAB-4174.

RNA sequencing

Worms were grown to L4 stage and total RNA was extracted using Trizol (Life Technologies) according to the manufacturer's description. For polyA RNA sequencing, the TruSeq Sample Preparation V2 Kit was used (Illumina). For RNA sequencing (mRNA, snoRNA,

tRNA and large ncRNA), a protocol has been described previously (Ikegami and Lieb, 2013). Briefly, total RNA was treated with DNaseI and depleted from rRNA with the Ribominus Eukaryote Kit (#A10837-08, Invitrogen). Fragmentation of RNA was performed using Fragmentation Buffer (#AM8740, Ambion) and cDNA was generated using the Superscript II Kit (Invitrogen). cDNA libraries were subjected to high-throughput single-end sequencing (50 bp) in an Illumina HiSeq 2500 instrument. RNA sequencing data was mapped to the WS220 genome reference using the TopHat 2.0.9 program (Kim et al., 2013) and gene annotation was derived from Ensembl release 66. All RNA sequencing has been submitted to ArrayExpress, under accession number E-MTAB-4172.

Immunofluorescence

Indirect immunofluorescence was performed using the ''freeze-cracking'' method (Duerr, 2006). Briefly, synchronized worms at L4 stage were fixed in 4% paraformaldehyde in 100 mM sodium phosphate buffer for 1 hr. Samples were washed three times with TBS-T for 10 min and blocked in 10% goat serum in antibody buffer (PBS, 0.5% Triton X-100, 1mM EDTA, 0.1% BSA, 0.05% sodium azide, pH 7.2) for 1 hr. Anti-FLAG primary antibody (#F3165, Sigma-Aldrich) was applied at a 1:100 dilution overnight at 4°C. The next day, samples were washed three times in antibody buffer for 20 min and incubated with the secondary antibody Cy5-labeled goat anti-mouse IgG (#A10524, Thermo Fisher) at a 1:500 dilution for 4 hr at room temperature. After washing with antibody buffer three times, samples were mounted in Vectashield mounting medium with DAPI (#H-1200, Vector Labs) and analyzed on a TCS SP8 laser scanning confocal microscope with a 40x/1.30 NA objective lens (Leica).

Filter retardation assay

The protocol was adapted from Wanker et al. (Scherzinger et al., 1997; Wanker et al., 1999). Briefly, crude worm lysates from synchronized L4 animals were resuspended in FTA sample buffer (10 mM Tris-Cl pH 8.0, 150 mM NaCl, 2% SDS) with protease inhibitors (Complete, Roche) and disrupted using a bead beater (FastPrep 24, MP Biomedicals) for 7 cycles of 20 s with 5 min rest in between cycles. Supernatants were transferred to new 1.5 mL tubes, and protein concentration was determined. To detect SDS-insoluble aggregates, 100 μg of total protein was mixed with 1 M DTT and FTA sample buffer (final concentration 40 μg/100 μl) and heated at 98°C for 5 min. Samples were filtered through a 0.22 micron cellulose acetate membrane using a 48-well Bio-Dot microfiltration system (Bio-Rad) and 100 μg of total protein was used for the assay plus two five-fold serial dilutions. Proteins were blocked for 30 min with 5% milk in TBS-T. Membranes were incubated with the primary antibodies α-GFP (#632381, Clontech Laboratories) or α-tubulin (#T6074, Sigma-Aldrich) at a 1:5000 dilution overnight at 4°C. Incubation with the secondary α-mouse antibody was at a 1:10 000 dilution for 1 hr at room temperature. Antibody binding was visualized with an ECL kit (#RPN2232, Amersham).

Co-immunoprecipitation

The protocol was adapted from (Ikegami et al., 2010). Briefly, crude worm lysates from synchronized L4 animals were resuspended in FA buffer (50 mM HEPES/KOH pH 7.5, 1 mM EDTA, 1% Triton X-100, 0.1% sodium deoxycholate, 150 mM NaCl) supplemented with protease inhibitors (Complete, Roche) and 1% sodium lauroyl sarcosinate (sarkosyl). Samples were cross-linked with formaldehyde for 30 min and 2.5 M glycine for 5 min. Worms were disrupted using a bead beater (FastPrep 24, MP Biomedicals) for 7 cycles of 20 s with 5 min rest in between cycles. Supernatants were transferred to new 1.5 mL tubes and protein concentration was determined. Lysates were pre-cleared for 30 min with Protein G-Sepharose beads (Amersham) and incubated with primary antibodies α-Pol II (#38520002, Novus Biologicals) or α-Pol III (#53330002, Novus Biologicals) at a dilution of 1:100 overnight at 4°C. Lysates were coupled to Protein G-Sepharose beads (Amersham) for 1 hr and washed five times for 5 min with FA buffer supplemented with 1 mM PMSF and protease inhibitor cocktail (Complete, Roche). Proteins were eluted by boiling the beads in SDS sample buffer and analyzed by western blotting.

Protein insolubility assay

Synchronized worms at L4 stage animals were resuspended in FA buffer and disrupted using a bead beater (FastPrep 24, MP Biomedicals) for 7 cycles of 20 s with 5 min rest in between cycles, followed by 15 sonication steps of 30 s with 30 s rest between cycles. Protein concentration was determined and equal amounts of lysates were incubated with 2% SDS for 1 hr at room temperature. The lysates were centrifuged at 13 300 rpm for 30 min and the supernatant (soluble fraction) was collected. The pellet (insoluble fraction) was washed two times with FA buffer and resuspended in urea buffer (8M urea, 2% SDS, 50 mM DTT, 50 mM Tris pH 8) for 1 hr. The samples were subsequently analyzed by western blotting.

Protein purification

Recombinant *moag-2/lir-3* was expressed and purified fused to the glutathione S-transferase (GST) from the pGEX-6-P1 vector in *E. coli* BL21 (DE) gold strain (Stratagene). Cells were grown in Overnight Express Instant TB Medium (Merck Millipore) supplemented with ampicillin (100 μg/ml) overnight at 30°C under constant shaking at 250 rpm. The cells were harvested by centrifugation, resuspended in lysis buffer (50 mM Tris pH 7.4, 150 mM NaCl, 1 mM EDTA and EDTA-Free protease inhibitor cocktail (Complete, Roche) and lysed by sonication. The cell debris was removed by centrifugation at 18 000 rpm (JA-25.50 rotor, Beckman Coulter). The supernatant was loaded onto a column containing Glutathione Sepharose 4 Fast Flow resin (GE Healthcare LifeSciences) and equilibrated with lysis buffer. The column was washed with 40 CV of lysis buffer and the protein was eluted in 50 mM Tris pH 8, 10 mM reduced glutathione and dialyzed in 50 mM Tris pH 7.4, 150 mM NaCl for the aggregation experiments.

Aggregation kinetics

4 μM solutions of GST-HttQ48 or GST-HttQ23 alone or with an equimolar concentration of *moag-2/lir-3* or *moag-4* were incubated in the presence of 7U of PreScission protease (GE Healthcare LifeSciences) per nmol of Htt protein in 50 mM Tris pH 7.4, 150 mM NaCl, 20 μM Thioflavin T at 37°C. The aggregation reactions were performed under constant linear shaking at 500 rpm and the ThT fluorescence was monitored in low-binding, clear-bottomed half-area 96-well plates. Emissions at 480 nm were recorded every 300 s with excitation at 440 nm, using a CLARIOstar plate reader (BMG Labtech). Fluorescence values were analyzed with the following sigmoidal equation:

$$y = A0 + \frac{A - A0}{1 + \exp(-(t - t50\%) * \mathrm{Kagg})},$$

where A_0 and A are the values at the beginning and the end of the aggregation, m_{A0} and m_A are the slopes of the lag phase and the plateau, assuming for them a linear dependency of normalized fluorescence values with the incubation time, $t_{50\%}$ is the midpoint of aggregation and k_{agg} is the apparent aggregation rate constant.

Subcellular fractionation

The protocol was adapted from (Chen et al., 2000). Briefly, crude worms lysates from synchronized L4 animals were resuspended in hypotonic buffer (15 mM HEPES KOH pH 7.6, 10 mM KCl, 5 mM $MgCl_2$, 0.1 mM EDTA, 350 mM Sucrose, 1 mM PMSF, 1 mM DTT, supplemented with protease inhibitors cocktail (Complete, Roche). Animals were homogenized using microtube pestle rods and motor (Kontes) by applying 10 strokes of 1 min followed by 1 min rest in between strokes. Worm debris was removed by centrifugation at 500 g for 5 min at 4°C. The pellet was discarded and the supernatant was used as input of the cell fractionation. Nuclei were pelleted at 4000 g for 5 min at 4°C. The supernatant containing the cytosolic fraction was centrifuged at 17 000 g for 30 min at 4°C to remove membrane fraction and contaminants. The nuclear fraction was washed two times with hypotonic buffer and resuspended in hypertonic buffer (15 mM HEPES KOH pH 7.6, 400 mM KCl, 5 mM $MgCl_2$, 0.1 mM EDTA, 0.1% Tween 20, 10% Glycerol, 1 mM PMSF, 1 mM DTT, supplemented with protease inhibitors cocktail (Complete, Roche)). The nuclear fraction was homogenized using 29G ± inch needle insulin syringe (Terumo) and treated with 25 U/μl Benzonase (Millipore) for 30 min at 4°C. Ten μg of each fraction was loaded on a 12% SDS-PAGE. Gels were transferred to nitrocellulose membranes (Brunschwig Chemie) and incubated with the primary antibodies α-FLAG (#F3165, Sigma-Aldrich) at a 1:1000 dilution; α-LMN-1 (#38530002, Novus Biologicals) at a 1:1000 dilution; α-GFP (#632381, Clontech Laboratories) and α-tubulin (#T6074-200UL, Sigma-Aldrich) at a 1:5000 dilution overnight at 4°C. Incubation with the secondary antibody was at a 1:10 000 dilution for 1 hr at room temperature. Antibody binding was visualized with an ECL kit (#RPN2232, Amersham).

Bioinformatic analysis

Conserved domains were identified using SMART (Simple Modular Architecture Research Tool) (Letunic et al., 2012; Schultz et al., 1998). Nuclear signal localization was predicted using NLS Mapper (Kosugi et al., 2009). Protein folding was predicted using FoldIndex (Prilusky et al., 2005). The algorithm used for motif discovery was the MEME Suite (Bailey et al., 2009). Orthologs were identified using protein BLAST search (https://blast.ncbi.nlm.nih.gov/Blast.cgi) and aligned with T-Coffee multiple sequence alignment tool (Notredame et al., 2000). Amino acid predictions were performed using ORF Finder (https://www.ncbi.nlm.nih.gov/gorf/orfig.cgi).

QUANTIFICATION AND STATISTICAL ANALYSES

Quantification of aggregates and motility assay

The number of aggregates present in whole worms was counted using a fluorescence dissection microscope (Leica). A minimum of 20 worms was counted and the data from three or four biological replicates were combined. For the motility assay, 15 animals were counted per experiment and the data from three biological replicates was combined.

A biological replicate was defined as an independently grown worm population, before extraction of embryos from gravid adult hermaphrodites to obtain synchronized populations (see Experimental Model and Subject Details). The exact number of biological replicates is indicated in the figure legends. Data are represented as mean ± SEM and significance was calculated using a one-tailed or two-tailed unpaired Student's t test. The exact type of Student's t test is indicated in the figure legend. *$p < 0.05$ **$p < 0.01$; ***$p < 0.001$.

RNA sequencing data analysis

All RNA seq are represented as the mean of n = 3 biological replicates, with error bars representing mean ± SEM. A generalized linear model was used to identify differential gene expression between the Q40 wild-type and the Q40 mutants with EdgeR (Robinson et al., 2010; McCarthy et al., 2012). Replicates 1-3 were introduced as a technical factor to correct for batch effect. Genes with average expression level below 1 fragment per million (FPM) were excluded from the analysis. The library normalization was left at the

standard setting (trimmed mean of M-values, TMM). The resulting p values were corrected for multiple testing using the Benjamini-Hochberg procedure. Per gene expression data was normalized as FPM. Data visualization and statistical tests were conducted using R scripts (available upon request).

Quantitative PCR analysis

All quantitative PCR are represented as the mean of n = 3 biological replicates, with error bars representing mean ± SEM. To measure the relative *lir-3* mRNA expression, *lir-3* transcript levels were quantitated using a standard curve of pooled cDNA solutions and expression levels were normalized against the endogenous reference gene *cdc-42*. To measure the relative Pol II or Pol III mRNA expression, the corresponding transcript levels were normalized to the expression of *rps-21* following the $2^{-\Delta\Delta CT}$ method (Livak and Schmittgen, 2001) (see Method Details).

Filter retardation assay

Immunoblots were quantified by densitometry using ImageJ (listed in Key Resources Table). To quantify the relative amount of SDS-insoluble protein, a ratio (fold change) was calculated by dividing the values of Q40;*moag-2/lir-3* mutants by their corresponding wild-types (corrected to α-tubulin as a loading control).

DATA AND SOFTWARE AVAILABILITY

The accession numbers for the ChIP-seq data reported in this paper are ENCODE: ENCSR408FDZ and ArrayExpress: E-MTAB-4174. The accession number for the RNA-seq data reported in this paper is ArrayExpress: E-MTAB-4172. Full images used in this study have been deposited to Mendeley Data and are available at http://dx.doi.org/10.17632/knzkvgbf6x.2.

Molecular Cell, Volume *65*

Supplemental Information

Identification of an RNA Polymerase III Regulator Linked to Disease-Associated Protein Aggregation

Olga Sin, Tristan de Jong, Alejandro Mata-Cabana, Michelle Kudron, Mohamad Amr Zaini, Francesco A. Aprile, Renée I. Seinstra, Esther Stroo, Roméo Willinge Prins, Céline N. Martineau, Hai Hui Wang, Wytse Hogewerf, Anne Steinhof, Erich E. Wanker, Michele Vendruscolo, Cornelis F. Calkhoven, Valerie Reinke, Victor Guryev, and Ellen A.A. Nollen

A

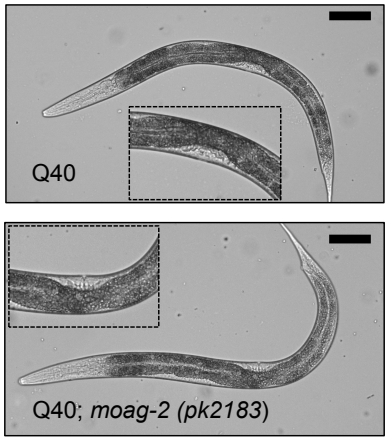

B

Reference	Variants	Gene	Amino Acid Change	Type of Mutation
C	T	*tag-124*	Ser89Phe	missense
C	T	*R05H5.4*	Gly155Arg	missense
C	T	*R166.3*	Asp50Asn	missense
C	T	*col-80*	Pro160Ser	missense
C	**T**	***lir-3***	**Met1Ile**	**loss of start codon**
C	T	*npp-3*	Ala1336Thr	missense

C

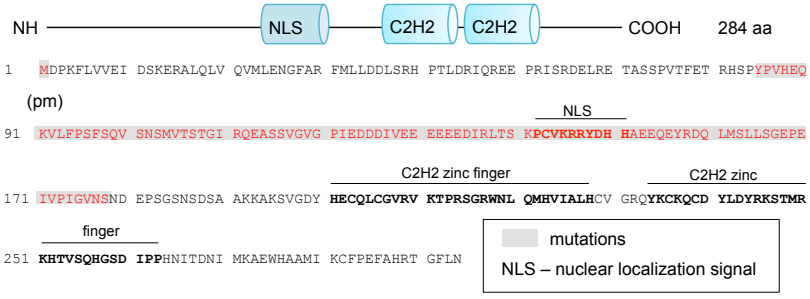

D

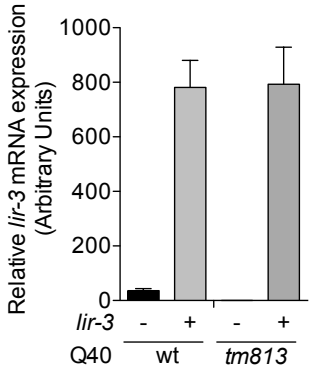

E

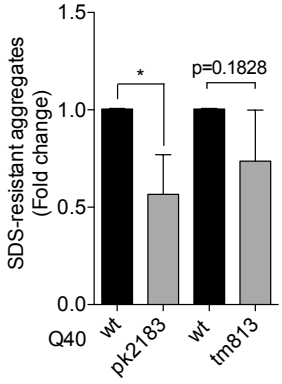

A

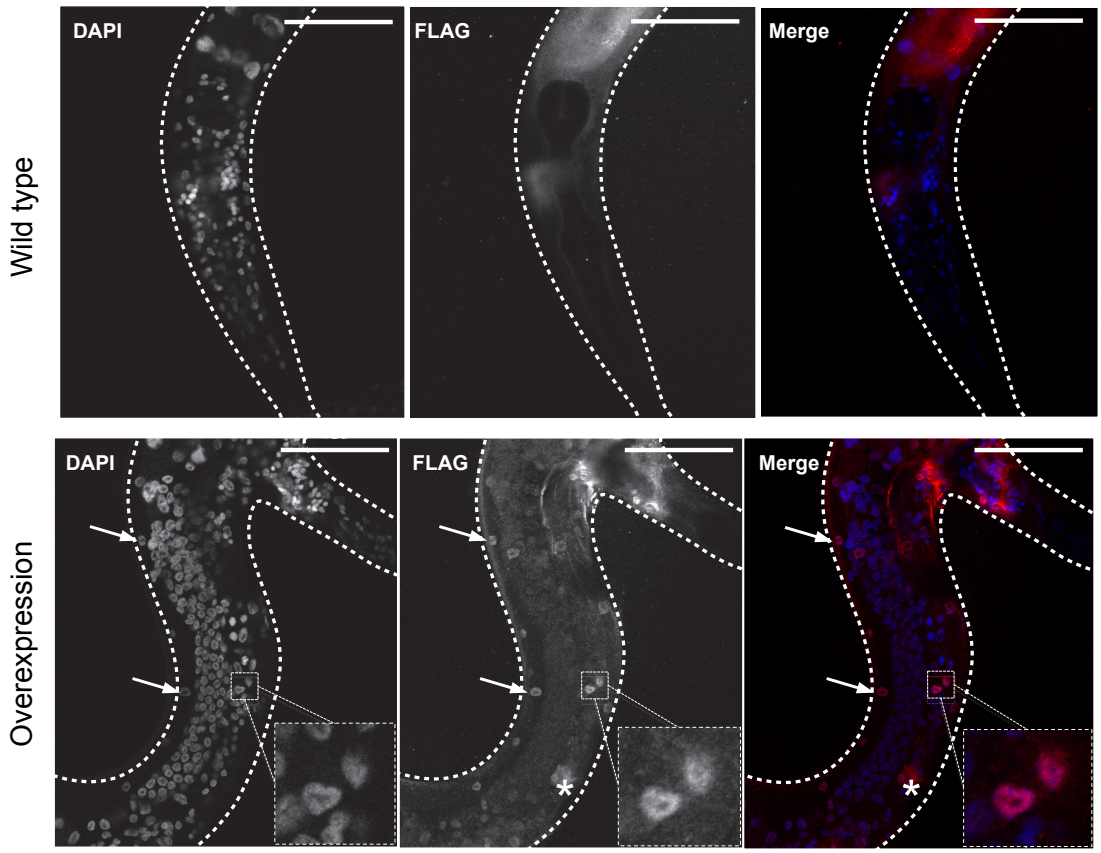

B

	MOAG-2/LIR-3 ChIP seq			Whole genome	
	Absolute	Relative (%)	P value	Absolute	Relative (%)
Protein coding	121	14.9	ns	20377	44.8
Pseudogene	13	1.6	ns	1431	3.1
ncRNA	300	36.9	ns	22753	50.1
rRNA	20	2.5	<0.001	20	0
snlRNA	0	0	ns	4	0
snoRNA	51	6.3	<0.001	139	0.3
snRNA	18	2.2	<0.002	114	0.3
tRNA	290	35.7	<0.001	609	1.3
Total	813	100		45447	100

A

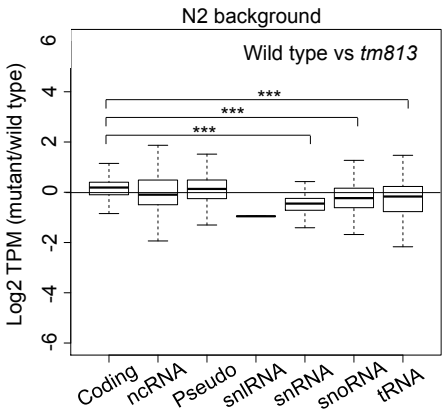

B

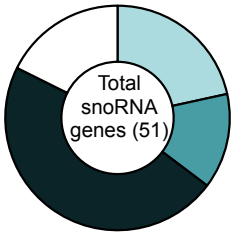

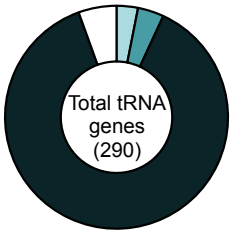

Box A (11)
Box B (7)
Box A and Box B (24)
Neither (9)

Box A (9)
Box B (11)
Box A and Box B (254)
Neither (16)

C

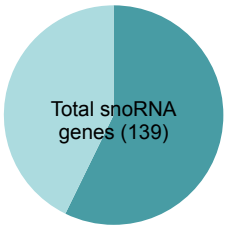

Genome
Pol II transcribed (79)
Pol III transcribed (59)

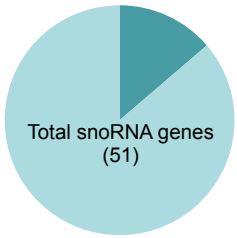

ChIP Seq
Pol II transcribed (7)
Pol III transcribed (44)

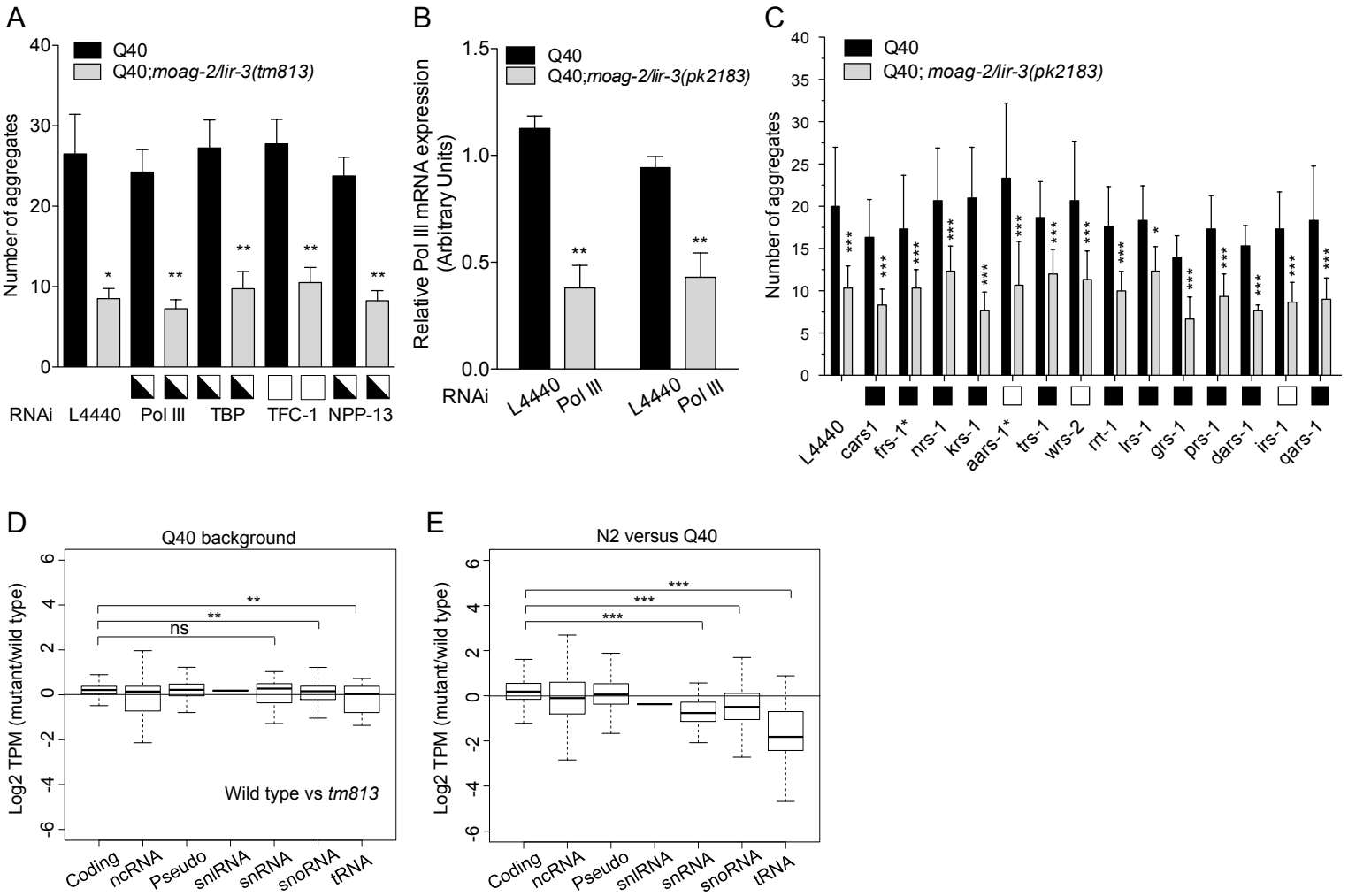
A
Q40
Q40;moag-2/lir-3(tm813)
Number of aggregates
RNAi L4440 Pol III TBP TFC-1 NPP-13
B
Q40
Q40;moag-2/lir-3(pk2183)
Relative Pol III mRNA expression (Arbitrary Units)
RNAi L4440 Pol III L4440 Pol III
C
Q40
Q40; moag-2/lir-3(pk2183)
Number of aggregates
L4440 cars-1 frs-1* nrs-1 krs-1 aars-1* trs-1 wrs-2 rrt-1 lrs-1 grs-1 prs-1 dars-1 irs-1 qars-1
D
Q40 background
Log2 TPM (mutant/wild type)
ns
Wild type vs tm813
Coding ncRNA Pseudo snlRNA snRNA snoRNA tRNA
E
N2 versus Q40
Log2 TPM (mutant/wild type)
Coding ncRNA Pseudo snlRNA snRNA snoRNA tRNA

A

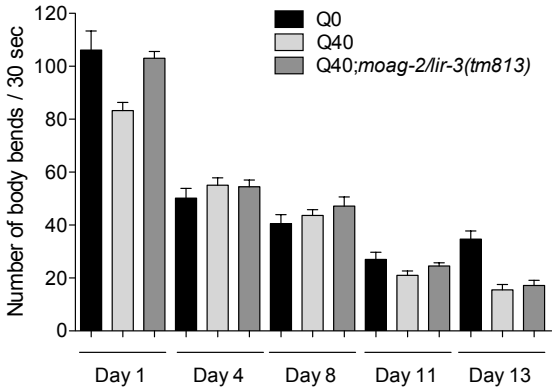

B

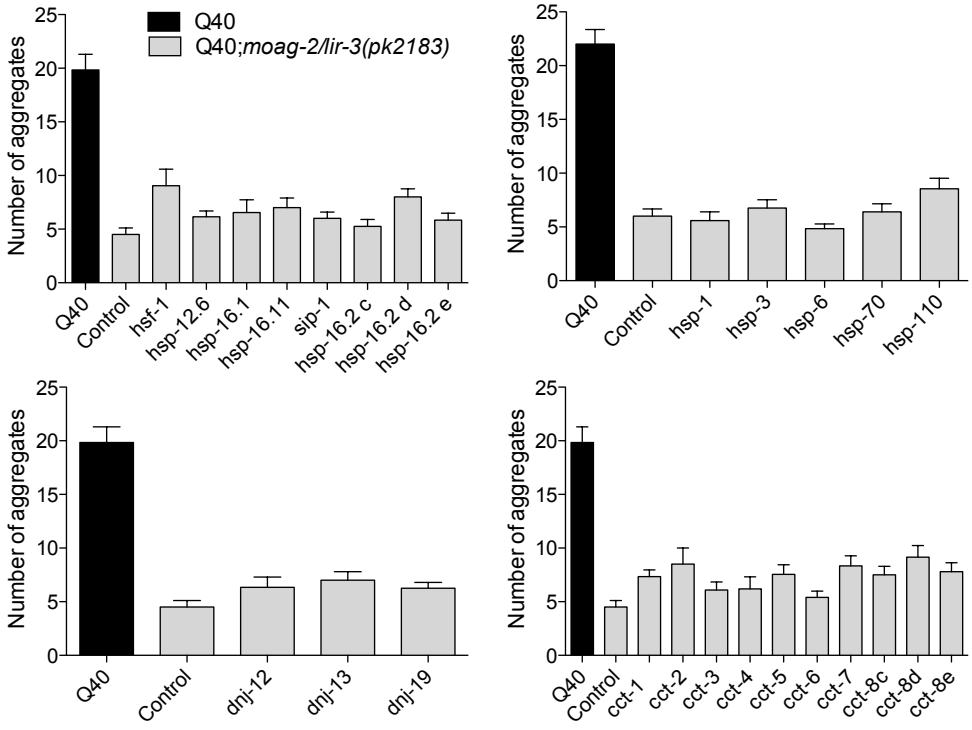

C

% Ratio Cytosol/Input			Fold change
	OE	Q40;OE	
Replicate 1	13.08	56.26	4.30
Replicate 2	4.26	71.35	16.74
Replicate 3	4.52	14.35	3.17

SUPPLEMENTAL FIGURE LEGENDS

Figure S1. Identification of *moag-2* as *lir-3* (related to Figure 1).
(A) Representative bright field images of L4-staged Q40 and Q40;*moag-2(pk2183)* worms. Insets show a magnification of the vulva. Scale bar, 75 μm.
(B) List of candidate genes for *moag-2* obtained by whole genome sequencing.
(C) Amino acid sequence of LIR-3 with the predicted nuclear localization signal (NLS, residues 132-141) and C2H2 zinc finger domains (residues 191-214 and 224-247). Grey shadow indicates location of the point mutation (pm) and the deleted residues in the *lir-3(tm813)* mutant.
(D) Transcript levels of *moag-2/lir-3* measured by quantitative PCR in Q40 and Q40;*lir-3(tm813)* worms from Figure 1E.
(E) Quantification of filter retardation assays by densitometry using ImageJ. The average of three biological replicates is represented. Data are represented as mean ± SEM and significance was calculated using a one-tailed unpaired Student's t-test. *$p<0.05$

Figure S2. Characterization of MOAG-2/LIR-3 as a nuclear protein that binds to the promoters of small ncRNAs (related to Figure 2).
(A) Subcellular localization of MOAG-2/LIR-3 in wild type N2 worms or worms overexpressing MOAG-2/LIR-3. Scale bar, 50 μm. Arrowheads point at nuclei; asterisks indicate non-specific staining.
(B) Number of MOAG-2/LIR-3 binding sites per gene biotype and total number of known *C. elegans* genes. The p values were calculated by permutation test.

Figure S3. MOAG-2/LIR-3 as a transcriptional regulator of small ncRNAs (related to Figure 3).
(A) Boxplot showing the relative expression of different gene biotypes in *lir-3(tm813)* relative to the wild type N2 background. Coding: protein-coding genes; ncRNA: non-coding RNA; Pseudo: pseudogenes; snRNA: small nuclear RNA; snlRNA: snRNA-like RNA; snoRNA: small nucleolar RNA; tRNA: transfer RNA. The average of three biological replicates is represented. ***$p<0.001$
(B) Number of MOAG-2/LIR-3 binding sites containing Box A and Box B in snoRNA and tRNA genes.
(C) Number of snoRNA genes encoded by Pol II or Pol III genome-wide and detected in this study.

Figure S4. Excluding the involvement of RNA homeostasis in polyglutamine-induced aggregation (related to Figure 4).
(A) Number of aggregates measured upon RNAi knockdown of individual components of the Pol III complex in Q40 and Q40;*moag-2lir-3(tm813)* worms.
(B) Transcript levels of Pol III measured by quantitative PCR in Q40 and Q40;*moag-2/lir-3(pk2183)* worms from Figure 4A.
(C) Number of aggregates measured upon knockdown of tRNA synthetases in Q40 and Q40;*moag-2/lir-3(pk2183)* worms. Asterisks indicate genes previously known to reduce protein aggregation. In panels A and C, an internal quality control for RNAi was performed and squares indicate penetrance (100% [closed]; 50% [half-open] and 0% [open]) of all associated visible RNAi phenotypes other

than aggregation. Aggregate counting was performed at the L4 stage. Data are represented as mean ± SEM and significance was calculated using a two-tailed unpaired Student's t-test.
(D-E) Boxplot showing the relative expression of different gene biotypes in Q40 and Q40;*moag-2/lir-3(tm813)* worms **(D)** and in N2 and Q40 wild type worms (Q40 wild type outcrossed from *tm813*) **(E)**. Coding: protein-coding genes; ncRNA: non-coding RNA; Pseudo: pseudogenes; snRNA: small nuclear RNA; snlRNA: snRNA-like RNA; snoRNA: small nucleolar RNA; tRNA: transfer RNA. *p<0.05; **p<0.01; ***p<0.001; ns is not significant. In all panels, the average of three biological replicates is represented.

Figure S5. Polyglutamine moves MOAG-2/LIR-3 to the cytosol where it turns into a positive regulator of protein aggregation (related to Figure 5).
(A) Number of body bends in Q0, Q40 wild type and Q40 worms overexpressing MOAG-2/LIR-3 (Q40;OE). One biological replicate is represented.
(B) Number of aggregates represented as fold change measured upon RNAi knockdown of cellular folding factors in Q40;*moag-2/lir-3(pk2183)* worms.
Aggregate counting was performed at the L4 stage and one representative experiment of three biological replicates is represented. Data are represented as mean ± SEM and significance was calculated using One-way ANOVA. ***p<0.001
(B) Quantification of the fraction of MOAG-2/LIR-3 present in the cytosol. The intensity of the bands was quantified using ImageJ. The FLAG signal in the input and cytosol were normalized against the signal for α-tubulin.

SUPPLEMENTAL TABLES

Table S1. Strains used in this study (related to Figures 1-5).

Strain name	Genotype	Source
N2 (Bristol)	wild type	
AM141	rmIs133[P(unc-54)Q40::YFP]X	Morley et al., 2002
OW1019	moag-2 (pk2183)	
OW1002	lir-3(tm0813)II	
OP312	wgIs312[P(lir-3)::TY1::EGFP::3xFLAG + unc-119(+)]	Sarov et al., 2006; Zhong et al., 2010
OW1009	mIs[P(unc-54)::Q0::YFP]V	
OW1021	rmIs133[P(unc-54)Q40::YFP]X	
OW1020	rmIs133[P(unc-54)Q40::YFP]X;moag-2(pk2183)II	
OW1004	rmIs133[P(unc-54)Q40::YFP]X	
OW1046	rmIs133[P(unc-54)::Q40::YFP]X; lir-3(het)II	
OW1003	rmIs133[P(unc-54)Q40::YFP]X;lir-3(tm813)II	
OW1096	rmIs133[P(unc-54)::Q40::YFP]X; zgEx221[P(myo-3)::CFP]	
OW1097	rmIs133[P(unc-54)::Q40::YFP]X; zgEx221[P(myo-3)::CFP]; lir-3(tm813)II	
OW1094	rmIs133[P(unc-54)::Q40::YFP]X; zgEx226[P(myo-3)::CFP + P(lir-3)::lir-3]	
OW1095	rmIs133[P(unc-54)::Q40::YFP]X; zgEx226[P(myo-3)::CFP + P(lir-3)::lir-3]; lir-3(tm813)II	
OW1059	rmIs133[P(unc-54)::Q40::YFP]X;[P(lir-3)::GFP::3xFLAG]	

Table S2. Overview and statistical analysis of aggregate counting experiments (related to Figure 1, 4, S4 and S5).
This table includes raw data showing the average number of aggregates and p values for the panel(s) in Figures 1, 4, S4 and S5.

Table S3. Analysis of differential expression between Q40 and Q40;*moag-2/lir-3* mutants (related to Figure 4 and S4).
This table includes raw data showing the changes in transcription between Q40 and Q40;*moag-2/lir-3* mutants in Figure 4 and S4).

Supplemental References

Morley, J.F., Brignull, H.R., Weyers, J.J., and Morimoto, R.I. (2002). The threshold for polyglutamine-expansion protein aggregation and cellular toxicity is dynamic and influenced by aging in Caenorhabditis elegans. Proc. Natl. Acad. Sci. USA *99*, 10417–10422.

Sarov, M., Schneider, S., Pozniakovski, A., Roguev, A., Ernst, S., Zhang, Y., Hyman, A.A., and Stewart, A.F. (2006). A recombineering pipeline for functional genomics applied to Caenorhabditis elegans. Nat. Methods *3*, 839–844.